NEW DESIGN FOR PRESSURE WASHER DRUMS

by

SUNNY CHI MAN FOK

B.A.Sc. (Mechanical Engineering), The University of British Columbia

A THESIS SUBMITTED IN PARTIAL FULFILLMENT OF
THE REQUIREMENT FOR THE DEGREE OF
MASTER OF APPLIED SCIENCE

in

THE FACULTY OF GRADUATE STUDIES
Department of Mechanical Engineering

We accept this thesis as conforming
to the required standard

The University of British Columbia

April 1997

In presenting this thesis in partial fulfilment of the requirements for an advanced degree at the University of British Columbia, I agree that the Library shall make it freely available for reference and study. I further agree that permission for extensive copying of this thesis for scholarly purposes may be granted by the head of my department or by his or her representatives. It is understood that copying or publication of this thesis for financial gain shall not be allowed without my written permission.

Department of Mechanical Engineering

The University of British Columbia
Vancouver, Canada

Date April 29, 97

DE-6 (2/88)

Abstract

In the kraft pulp and paper industry, pressure washer drums are used to separate bleaching liquor and chemicals from pulp. These drums have experienced serious structural damage in terms of cracks in critical areas that have led to excessive production down time of the washers. In this thesis, a new mechanical design for these washers that eliminates problems in the original design and greatly extends the life of the equipment is presented. The first part of this thesis discusses finite element simulation and experimental testing of the current and the proposed new design whereas the second part of the thesis discusses the design optimization and fatigue life prediction of the new design using finite element sub-modeling technique. The final part of the thesis investigates special start-up procedures that minimize the thermal shock effect on the new design.

The development of the new design starts by numerically simulating the existing washer drum design in an attempt to predict real life observations for such drums. This process involves experimental testing of a full scale drum in order to assess the load carrying capacity of various parts of the drum and to identify key boundary conditions for use in the finite element computer model. Various design modifications are then studied and numerically assessed. Shape optimization is then carried out for a specific area in the final design. A prototype was built based on the final model and experimental testing was performed in actual operating conditions.

In order to numerically assess the fatigue life of the new design, the growth rate of a fatigue crack located at the critical area is investigated and presented in the second part of the thesis. The procedure involves putting a crack in the finite element model of the new design

rather than using a standard or 'can-model'. The stress intensity factors are then calculated for the crack under actual loading conditions and with the actual geometry of the structure. Various crack lengths are considered and a plot of the variation of the stress intensity factor (SIF) with the crack length is obtained. Displacement extrapolation method is used to calculate the SIF at the crack tip. The fatigue life cycle of the structure is then estimated based on the calculated SIF and Paris law. Comparison of this detailed and more accurate procedure with the standard 'can model' procedure is given.

In the final part of the thesis, a detailed transient heat transfer analysis is performed to predict the temperature distribution in the structure during start-up and shut-down stages. Based on the predicted temperature distribution and the corresponding thermal stresses, a start up procedure is proposed with the objective of minimizing both the impact of thermal shock as well as the time required for start up.

Table of Contents

List of Figures

Acknowledgments

I would like to thank my supervisor, Dr. Mohamed Gadala, for his great support and guidance. Without his help, my research and this thesis will not have been completed.

I would also like to thank Tristar Industries Inc., Domtar Packaging, and Potlatch mill for the financial support for my study, and the assistance they offered for carrying out the experimental testing performed for this research.

Chapter 1

INTRODUCTION

1.1 BACKGROUND

Paper pulps undergo a wide range of processing steps, depending on their method of preparation (i.e., mechanical, semi-chemical, chemical virgin pulps) and their end use. Screening, thickening and storage operations are necessary for virtually all pulp grades, while cleaning is usually required where appearance is important. Defibering is required for all semi-chemical and high-yield chemical grades. Screening, defined as removal of irregular shaped wood pieces and oversized or uncooked chips, is usually necessary in the production of clean bleachable chemical pulps. Pulp drying is required when pulp is stored for long periods of time (to prevent fungal or bacteriological activity) or shipped over considerable distances (to reduce weight and thus freight costs). A schematic flowchart illustrating the sequence of processing steps for a typical kraft mill operation is shown in Figure 1.1.

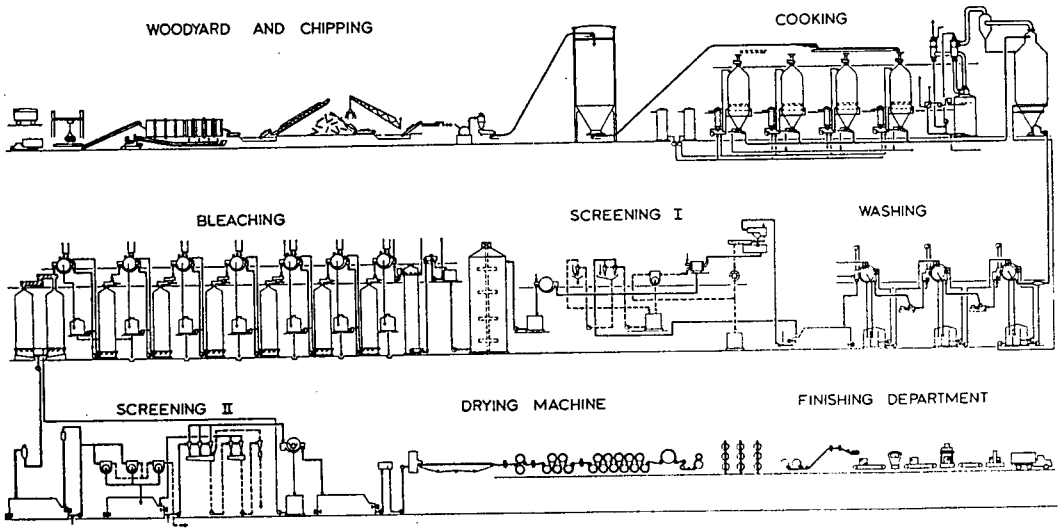

Figure 1.1: Schematic flowchart for a kraft mill operation

As indicated in the figure, logs are first reduced to chips and then chips are *cooked* in *digesters* in order to break them down to finer fibers. In the cooking process, the digester vessel is filled with chips and liquor is added to cover the chips. The contents are then heated according to a predetermined schedule, usually by forced circulation of the cooking liquor through a heat exchanger. After digestion, the softened chips are disintegrated into fibers. The cooked pulp is then transported to the washing process (brown stock washing) to dilute and remove the residual cooking liquor. The washed pulp is screened to filter out unwanted particles and then bleached to remove unwanted colors. After going through a second screening process, the pulp proceeds to the drying and rolling machines and finally the baled product is routed for further processing into paper related products.

In the brown stock washing process, the cooked pulp from the digesters must be washed in order to remove dissolved organic and soluble inorganic material present in the pulp that would contaminate the pulp during subsequent processing steps, and to recover the maximum amount of spent chemicals with minimum dilution [1-3]. Various types of washing equipments are used in this process. The washing equipments may be rotary vacuum, pressure washers, press washers, dilution/extraction equipment, horizontal belt washers or core pipe disc filters. Multiple stage vacuum and pressure washers constitute the vast majority of systems currently operating in North America [2].

The main component of a vacuum washer (refer to Figure 1.2) is a perforated cylindrical shell or deck that rotates in a big container or a vat containing the pulp slurry. By means of internal valving and a sealed dropleg, vacuum is applied as the rotating drum enters the stock. A thick layer of pulp builds up and adheres to the perforated drum surface as it emerges from the vat. Wash water is applied to displace the residual liquor in the pulp mat

formed on the drum surface and the low pressure inside the drum enables sucking residual liquor from the pulp mat as the drum continues to rotate. Finally, the vacuum is cut off and the washed pulp is removed from the mold. The average efficiency of displacement for a single stage vacuum washer rarely exceeds 80%, due to a number of factors. Consequently, three or four stages are required to attain an overall satisfactory removal of the washable liquors.

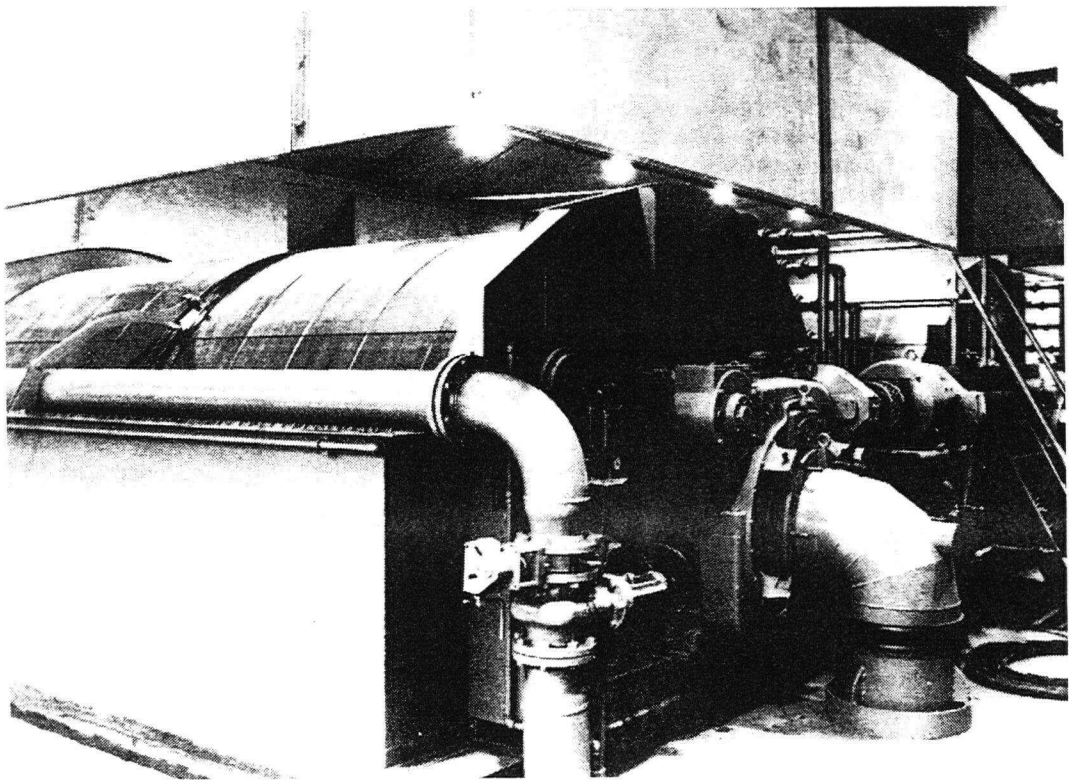

Figure 1.2: Brown stock vacuum rotary washer

Rotary pressure washers are similar in operation to rotary vacuum washers, but appear to offer some significant advantages. A picture of a pressure washer drum is shown in Figure 1.3. The pulp mat is formed on the surface of the cylinder or the drum deck (see Figure 1.4) in a way similar to the vacuum washer. The pulp mat is dewatered with the aid of pressure applied on the outside surface of the drum face in a specific area normally called

the 'forming board', as opposed to vacuum inside the cylinder in the vacuum washers. Because the driving force for pulp mat formation, dewatering, and wash liquor displacement is applied outside the drum, the interior of the washer drum can be utilized for a more sophisticated liquor collection system.

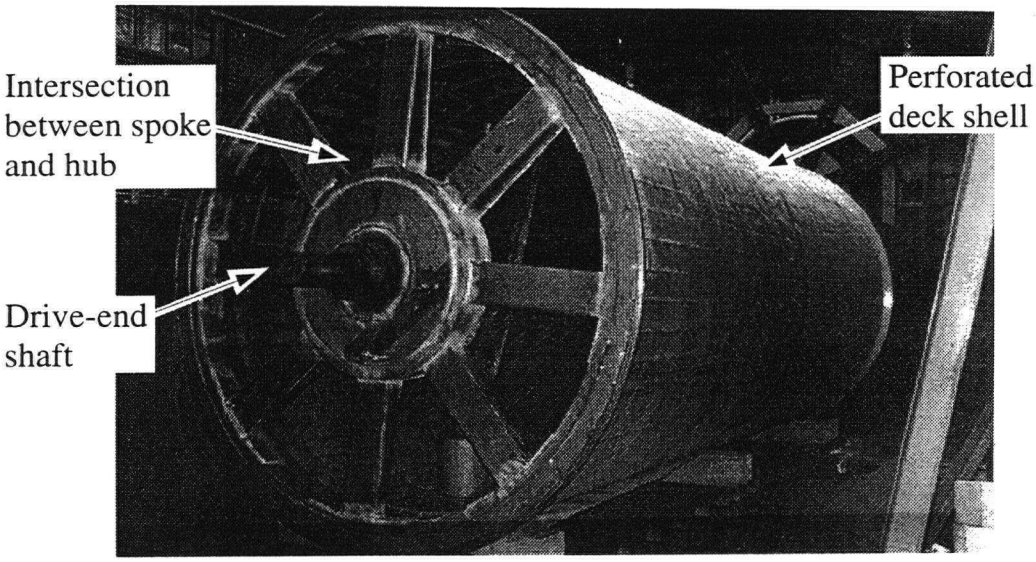

Figure 1.3: A pressure washer drum

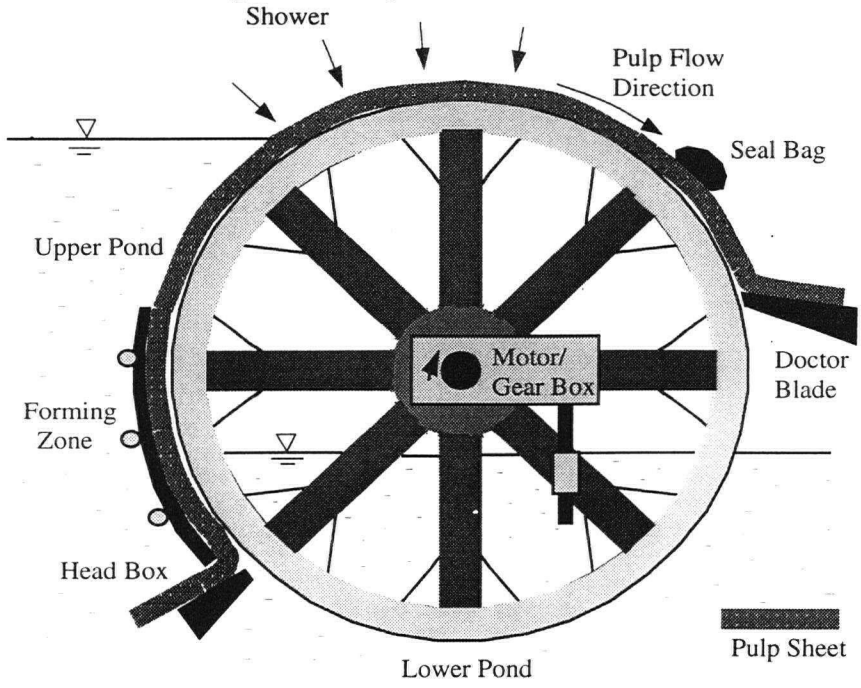

Figure 1.4: Operating procedures of a pressure washer

The relatively high pressure on the drum face, compared to vacuum washer, facilitates relatively higher efficiency for pressure washers. Also, the relatively high pressure inside the washer housing also allows higher temperature wash liquor to be used which greatly reduces foaming. The closed vapor circulation system also facilitates collection and treatment of odorous vapors.

1.2 PROBLEM STATEMENT AND OBJECTIVES

Although pressure washer drums operate at a relatively low speed, (1-3 rpm), they operate under a hostile environment of corrosion from the chemicals involved in washing, and a relatively high structural loading [4]. From the mechanical side, the primary structural load in a pressure washer drum is from the process pressure in the forming board area and the input torque required to operate the drum. The secondary loads are frictional forces, reaction forces of the drive mechanism, drum weight and thermal stresses specially during start-up and shut-down procedures.

Many uncertainties arise in the design process of pressure washer drums. The calculations of accurate loading conditions that the drum may experience is a major concern. Such conditions are complicated by practical considerations of occurrence of stall situations which the drum's rotation is actually stalled by the pulp built up on the drum surface. Assessment of the hostile environment conditions and its impact on the material properties and fatigue characteristics of the drum pose another important concern in the design process. Another consideration is the impact of the fabrication process and welding procedures and welding locations on the resulting residual stress in the drum before operation [5].

The impact of the above uncertainties in the design process is probably evident in the frequent failures of such pressure washer drums after a relatively short period of

operation, 1-2 years. Figure 1.5 shows one of the most common cracking areas, which is the spoke and hub intersection on the drive-end of the existing washer drums. Some of the above mentioned concerns for load assessment are discussed in chapter 2. The finite element modeling, details of the analysis and re-design of the drum as well as finite element shape optimization for specific areas in the drum design are presented in chapter 2 and 4, respectively. Experimental testing to assess loading conditions on the drum in the initial design stage and to validate model results in the final stage of the design is discussed in chapter 3.

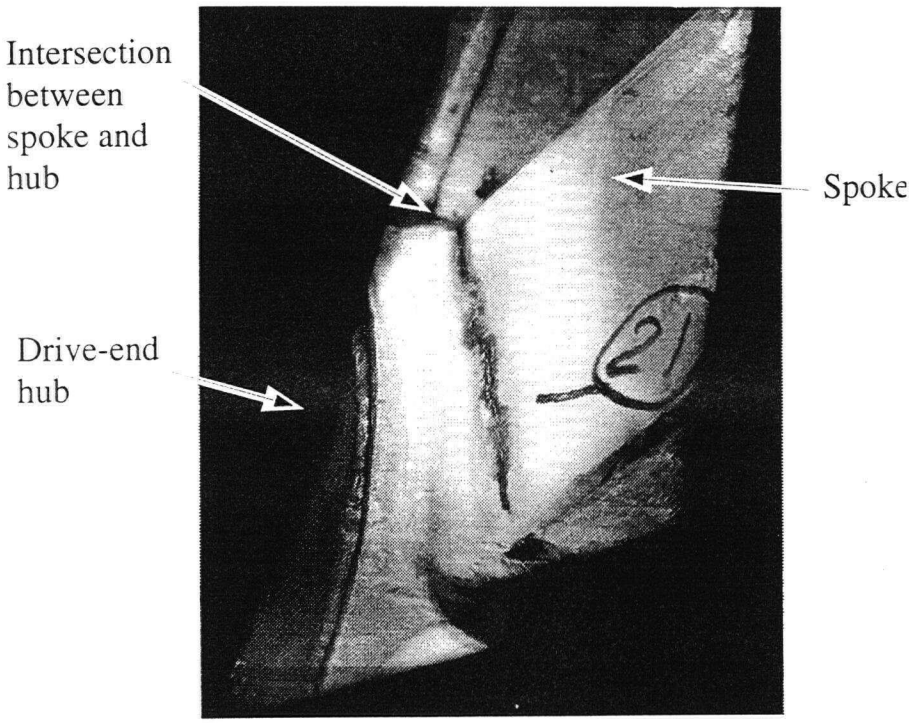

Figure 1.5: Cracking in the existing pressure washer drum

In the second part of this research, chapter 5, service life of the existing and the new design is compared based on the stress results obtained from the finite element simulations. The crack propagation rate of the new design is computed using two different methods: a simplified numerical model (can-model) under alternating stress range obtained from regular

finite element analysis of the structure without a crack; and a detailed finite element sub-modeling technique which involves putting a crack in the finite element model of the new design and calculating the stress intensity factors for the crack with various crack lengths in the actual geometry. The displacement extrapolation method is adopted and the fatigue life cycle of the structure is estimated based on the calculated stress intensity factors.

In the final part of the thesis, chapter 6, heat transfer analysis and thermal stress analysis for the new design in the normal start-up process is studied. During the normal start-up process of pressure washers, the drum needs to be heated up to its normal operating temperature of about 100°C (210°F) in a short period of time, usually 15 minutes to 30 minutes. One of the concerns is that this sudden heating may generate high thermal stresses in the drum or thermal shock loading to the drum structure. This is important especially in the region near the intersection of the stainless steel plates and the large solid hub area since the steel plates used in the structure tend to heat up more rapidly compared to the thick solid hub. In this section, the thermal stresses caused by the general start-up procedure are investigated using a finite element transient heat transfer analysis and various heat-up curves are tested and investigated. An optimized heat-up procedure that minimizes the impact of these stresses is developed and proposed based on the analysis performed.

Chapter 2

STRESS ANALYSIS USING FINITE ELEMENT METHOD

2.1 FINITE ELEMENT MODELING OF THE WASHER DRUMS

2.1.1 Introduction

The finite element method is a numerical analysis technique for obtaining approximate solutions to a wide variety of engineering problems. Although originally developed to study the stresses in complex airframe and civil engineering structures, it has since been applied to the broad field of continuum mechanics as well as other fields of engineering. Because of its diversity, flexibility as an analysis tool and the availability of reliable commercial programs utilizing the method, it is receiving much attention in industry [6,7].

In any body of matter (solid, liquid, or gas) having arbitrary dimensions and shape, the field variable (displacement, stress, pressure or some other quantities) possesses infinitely many values because it is a function of each generic point in the body. Consequently, the problem is one with infinite number of unknowns or degrees of freedom. The finite element discretization or modeling procedures reduces the problem to one with a finite number of unknowns by dividing the solution region into small but finite *elements* and by expressing the unknown field variable in terms of assumed approximation functions within each element. The approximating functions, or more commonly known as *shape functions*, may be defined in terms of the values of the field variables at specified points on the element boundary called *nodes* or *nodal points*. The nodal values of the field variable and the approximation functions for the element completely define the behavior of the field variable within the element.

Finite Element Analysis (FEA) has become a popular choice of practicing engineers to solve real life problems for stress, vibration, deformation and other field problems due to the increasing popularity of powerful computers and finite element commercial packages, see for example references [8] and [9], which can handle a large number of equations in a reasonable period of time. A general finite element software package provides the necessary tools to perform such analysis for a wide variety of problems without compromising accuracy. Every commercial finite element software is basically comprised of three components: the pre-processor, the solver and the post-processor [8,10]. The pre-processor enables the designer to model and simulate the physical problem into a geometric and finite element data base. The solver basically calculates the model equivalent stiffness and solves the system equilibrium equations. Finally, the post-processor performs results manipulation and display.

2.1.2 The Drum Models

The following stages are performed in the modeling and the design optimization of the pressure washer drum:

- Build an accurate FE model for the existing drum design and perform model testing and verification load cases.
- Perform experimental testing on the existing drum in order to make proper modeling decisions and assess the actual loading and boundary conditions.
- Run the drum model under various operating conditions. Refine and fine tune the model to predict real life findings observed from drums in service.
- Identify and study various design modifications and provide qualitative assessment to each one. This may be performed through static and/or fatigue runs for each proposed design modification.

- Perform design optimization finite element analysis for specific areas of the drum to optimize the designed shape. Weight and cost of the component are the primary objective functions for the optimization process.
- Build a prototype for the proposed design and perform experimental testing in actual operating conditions to verify model results.

In the first stage, building a FE model of the existing drum, it is important to realize the impact of the results of this step on other steps of the design process. The drum model should represent all details of the drum with appropriate accuracy to predict stress levels. It is decided, at this early stage, to build a full drum model and not to use sub-models for various parts of the drum. This is felt more appropriate and more accurate since it eliminates the uncertainties involved in specifying boundary conditions on the pertinent sub-model. Behavior of areas with highly localized stress risers, e.g. welds and around small holes, may not be accurately represented, however, by the global model. For such areas, appropriate stress concentration factors or localized sub-models are considered. By inspecting various failure cases of existing drums, specific areas of concern are identified as: shaft to end-plate welds, spoke to hub intersection and spoke to deck intersection. Refer to Figure 1.3 and 2.1 for identification of these areas and for general description of the drum model. In the existing drum model, approximately 9,000 elements and 33,000 degrees of freedom (DOF) were used to model the existing 8.13 m (320 in.) long and 3.43 m (135 in.) diameter pressure washer drum. As shown in Figure 2.1, the model contains most of the geometric details of the actual drum: a shell with equivalent density and Young's modules (simulating the perforated plate, see Appendix-1 for details); 8 tapered spokes at each end of the drum; longitudinal reinforcement members and 15 fly rings; 2.54 cm (1 in.) shell elements modeling

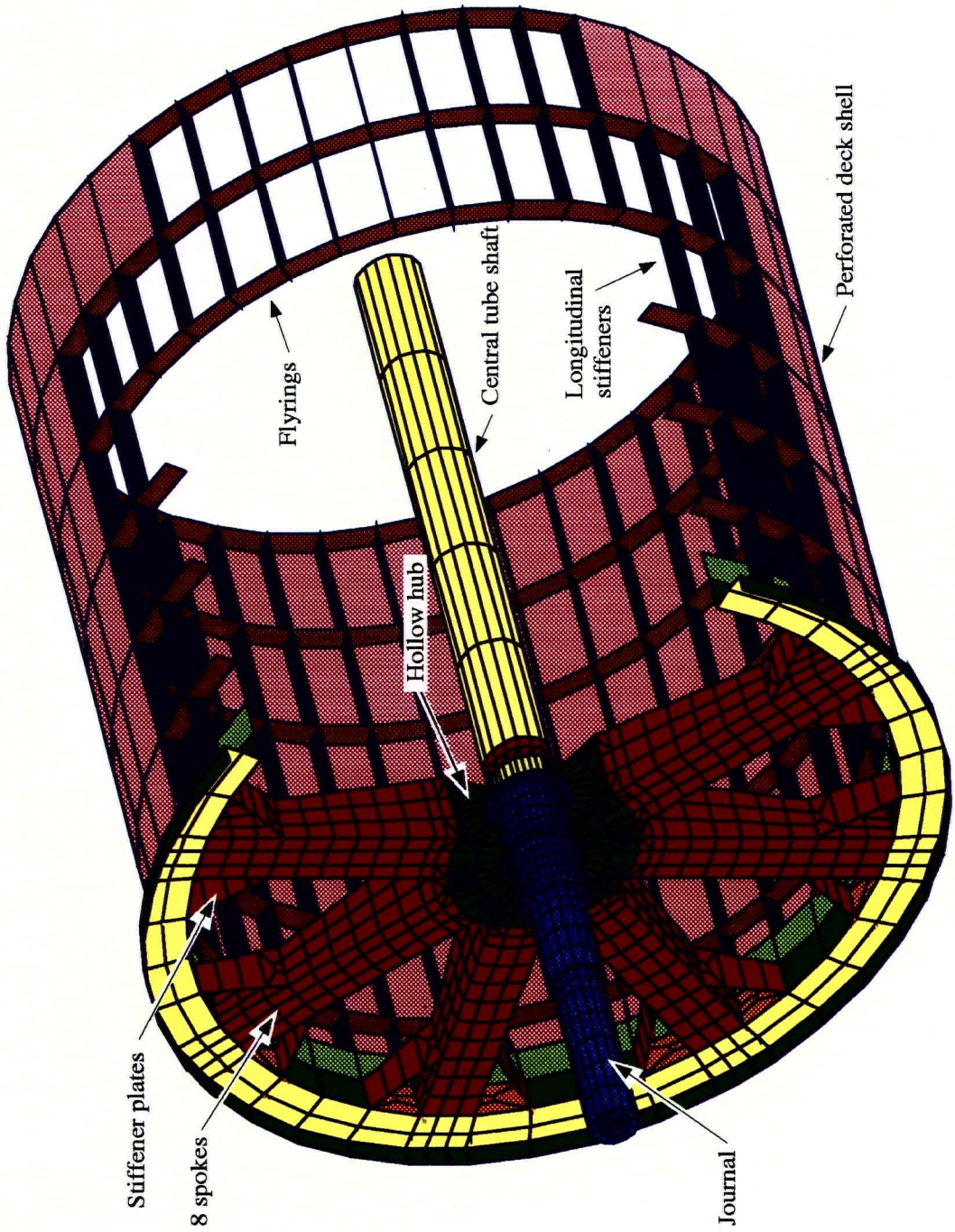

Figure 2.1: The existing washer drum design

the hub plates and three dimensional solid elements modeling the shaft at the drive and idle-ends. The liquor collecting trough is reduced to two sets of force vectors representing the weight of the trough and the liquor.

After geometric and FE model checking with various standard checks available in the NISA program [8], various sample test cases were applied to the model for assessment of performance. The independent load cases applied were: simple tension at one end of the drum; simple bending at the mid-span; weight of the drum as body force and an external uniform pressure on the deck surface. Results of all cases were compared to simple hand calculations and proved the adequacy and correctness of the model.

2.1.3 Boundary Conditions

The pressure washer drum sits in the washer housing called the vat. One side of the vat has a separate tank called the upper pond containing pulp slurry and providing hydrostatic pressure on the drum face. The same side of the drum has a shoe-like board called the forming board through which pulp slurry is fed to the drum surface under relatively high pressure, refer to figure 1.4 for details. As the drum rotates, the pulp mat starts to form in the forming board area and is then carried along the upper deck surface of the drum. High pressure water jets, located above the top of the drum, displace the unwanted chemicals through the perforated deck shell of the drum to the lower pond. The washed pulp mat is then peeled off from the drum surface by the use of a sharp peeling blade facing the drum surface called the doctor blade. The process is shown schematically in Figure 1.4. The actual loading and constraints on the drum model are composed of the following main components:

- Input drive torque.
- Surface or deck pressure and frictional forces: These are due to the forming board, slurry tank pressure, shower pressure, pulp mat, doctor blade, and other small components used for sealing, namely seal bags and seal cables.
- Body forces due to weight of the drum and trough.
- Reaction forces from the motor-gear box assembly.
- Displacement constraints at the two ends of the drum to simulate bearing supports.

Among the above list of loading and constraint conditions, the forming board pressure and friction forces, pose a major uncertainty in the design process. This uncertainty is due to the lack of any reliable data for the pressure distribution inside the forming board, pressure and friction due to seal bag and doctor blade and tension on the seal cables. Numerical test cases (refer to Figure 3.7 for sensitivity test results) show that such pressure distribution has a major effect on the stress distribution in the drum. Another area of concern is the method by which the torque is absorbed or equilibrated on the drum surface and the center shaft, i.e. the distribution of the torsional reactions counter balancing the input torque. Also, it is required to provide an assessment of the effect of changes of the drum surface pressures on the torque transmitted through the shaft to the idle end of the drum. In order to eliminate some of the above concerns, a full-scale experimental test was performed on an actual drum. The experimental set-up for the above task will be discussed in chapter 3 of this thesis. In the loading specifications and assumptions described in the following, various findings and conclusions from the performed experiments are utilized.

Three main static load cases are considered as follow:

- The normal operating condition which will be referred to as level-3 torque.
- The 'dirty' operating condition which will be referred to as level-5 torque.
- The stall condition which will be referred to as level-20 torque.

In the following, more details of the handling of various loads and boundary conditions applied to the drum model are addressed:

Input torque

In the FE models, the input torque is applied to the journal drive-end as uniformly tangential forces on the outer radius of the drive shaft (see Figure 2.2) and the following simple torque equation is used:

$$T_{input} = \sum_{i=1}^{n} r \cdot F_i \tag{2.1}$$

where r is the radius of the drive-end shaft, F_i is the force acting tangential to the shaft cross section, and n is the number of nodes along the circumference of the drive-end shaft.

Input torque values were measured on existing drums under actual service conditions. The values of the input torque obtained and used in the FE models are: 71.2 kN.m (630,000 lb.in.) for the level-3 torque; 129 kN.m (1,141,000 lb.in.) for the level-5 torque and 561.5 kN.m (4,969,000 lb.in.) for the level-20 or the stall torque condition. The nodal force vectors for nodes at the bottom section of the shaft are combined with the reaction forces of the motor-gear box assembly.

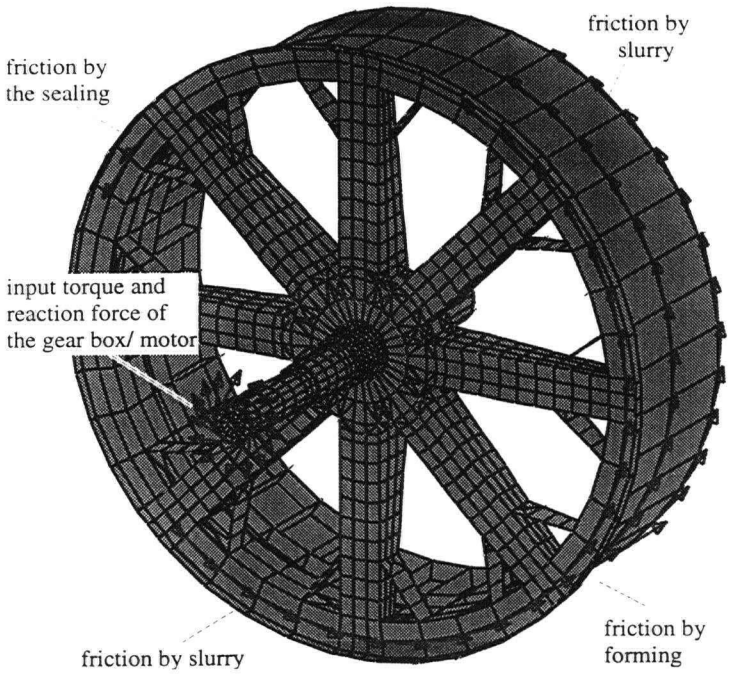

Figure 2.2: Nodal forces applied to the FE model of existing drum design

Pressure on the drum surface:

The upper section of the drum deck is under the pressure given by the water showers while some other parts of the drum are under hydrostatic pressure from the pulp slurry, see Figure 2.3 for details of pressure distribution on the drum surface. The more significant pressure loading on the drum surface comes from the pressure in the forming board zone.

The experiment performed on the actual drum (details will be discussed in chapter-3) in service provides pressure values at sample pressure points in the forming board area and those are used to approximate the pressure distribution. From the pressure values obtained experimentally, an assumption was made that the frictional torque due to the pressure in the forming board area is contributing 70% of the total friction torque on the drum surface. Sensitivity runs were performed to check the impact of changing this percentage on the final stresses in the drum and it was found that the 70% assumption gives the worst case scenario.

The sensitivity runs also showed that changes in the friction distribution on the drum surface in the axial direction do not have a significant impact on stresses in the key areas of concern.

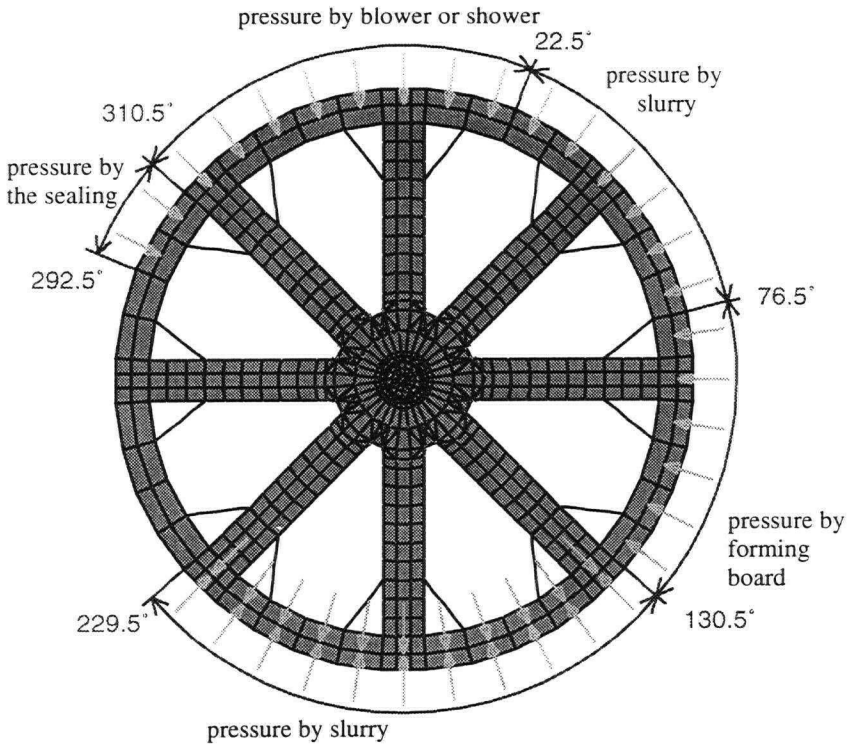

Figure 2.3: Pressure applied to the FE model of the existing drum design

Frictional forces:

It is assumed that the torque input will be consumed entirely by the friction acting tangentially to the drum surface (counteracting the input torque) and, therefore, there is no torque transmitted to the idle-end of the shaft (see Figure 2.2 for friction force distribution). The frictional force on the drum surface is calculated as simple coulomb friction in relation to the applied pressure:

$$F_f = \mu \cdot A \cdot P \qquad \text{and} \qquad \sum F_f \cdot R = T_{input} \tag{2.2}$$

where:

μ is the local coefficient of friction, A is the local area (area of the element), P is the local pressure on the element surface, R is the radius of the drum, and T_{input} is the input torque.

As discussed above, approximately 70% of the torque due to friction on the drum surface is assumed to be in the forming board area. It is further assumed that the friction in the slurry tank area will contribute about 25 % of the total friction force with the remaining 5% contributed by the seal bag and doctor blade areas. To achieve this result, the local coefficients of friction for the doctor blade / forming board areas are computed to be 0.15 and it is 2.5 times the coefficient of friction of the immersed areas in the slurry tank.

A spread sheet was generated to calculate the magnitude of the frictional forces that counteracted a specified input torque and cancelled it entirely at the idle end of the drum. The program calculates pressure values based on coordinates and location of nodal points (i.e., upper pond, lower pond, forming board or shower area), element areas and centroid and friction force vector due to pressure on the element face. By inputting the operating parameters such as input torque, ratio of friction coefficient of different areas, the spread sheet program calculates the force vector applied to each node point on the drum surface. The program also computes the overall and local coefficient of friction on the drum surface.

Body force:

The weight of the drum is assumed to be the only body force. Since the drum rotation is very slow (1-3 rpm), the inertia forces are assumed negligible and are not considered in the analysis.

Reaction force of motor/gear box:

The input torque is generated by a motor assembly and is transmitted to the drive end through a gear box. This gear box assembly is designed to be hanging on the drive-end shaft.

Considering the combination of the weight of the motor/gear box and the torque input, a reaction force acting on the drive-end shaft results.

Displacement constraint:

Since it is assumed that no torque is transmitted to the idle-end, displacement and rotation of all circumferential nodes at this end are constrained whereas only a point on the axis of the shaft on the drive-end is constrained to allow rotation of the drive-end shaft. The circumferential reaction forces on the nodes at the idle-end are checked to make sure the torque is balanced.

2.1.4 Design Modifications

In this stage, a series of trial models were built with increasing number of degrees of freedom (DOF) to gain insight into the behavior of the model and to make an assessment of the proper mesh density required for the analysis. Each of these models was tested with simple load cases and the results were assessed in a comparative manner. Attention was drawn to finding the optimal element mesh size in the end-plate, web-plate and hub area. Element distortions were also investigated and minimized. Final constructed and tested models ranged in size from 17,000 elements and 85,000 DOF to 30,000 elements and 130,000 DOF with a maximum wave front of 4000 DOF (after wave front minimization). The finite element models built in this stage included all proposed design modifications for the drum. These modifications were modeled in such a way that they may be implemented in an incremental manner in order to assess the merits of each one individually. In the following, the main design modifications considered for the new design are summarized:

- An end-plate sandwich structure with 16 web-plates welded in-between the two end-plates with 16 drainage openings on each: This provides a much higher bending and torsional stiffness to the end-structures due to the newly proposed sandwich structure form.
- A solid hub/ flange combination (journal) on the drive as well as the idle end of the drum.
- A sandwich structure upper-deck or cage in the critical transition area between the end-plates and the upper deck.
- A central hollow shaft resting in the hub assembly at both ends of the drum.

The details of the existing and the final new hub designs are given in Figure 2.4 and 2.5, respectively.

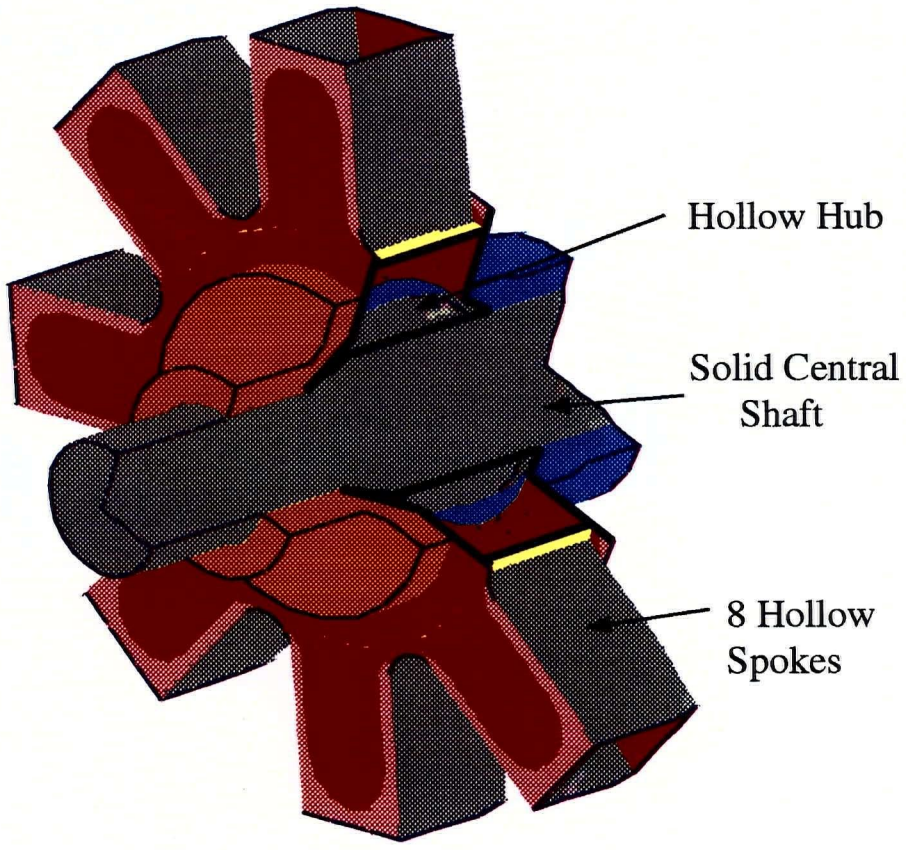

Figure 2.4: The existing hub design

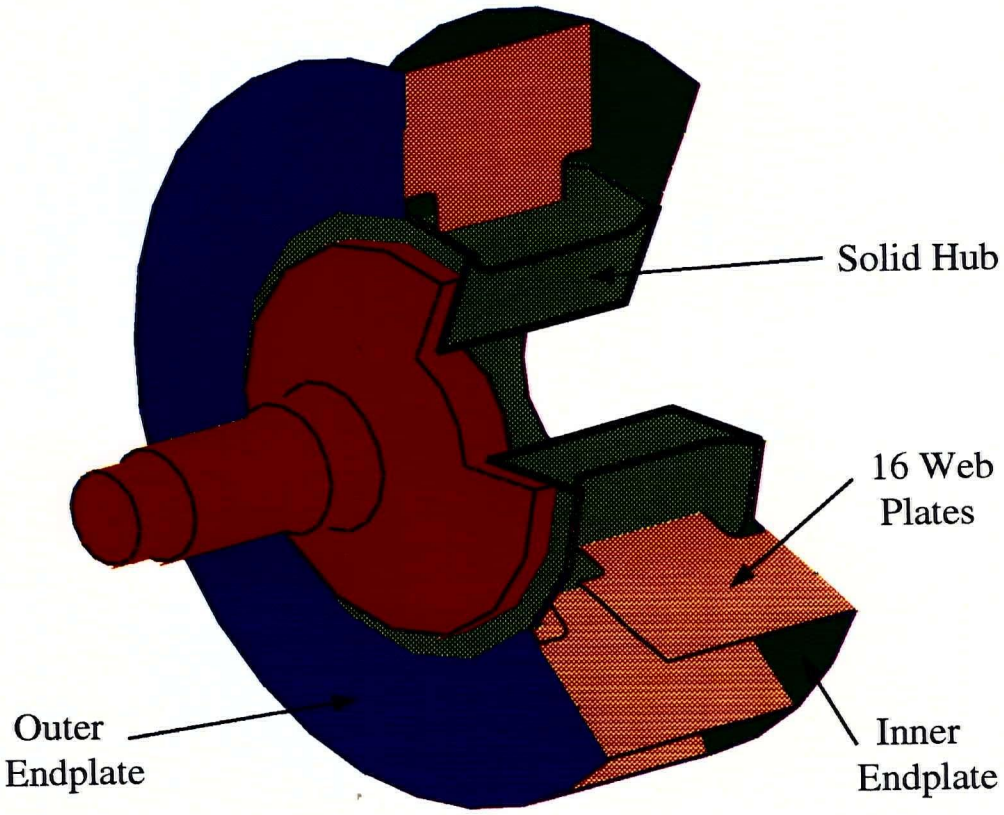

Figure 2.5: The new solid hub design

The above modifications represent the final ones for the modified design. They have been arrived at after studying and modeling numerous intermediate design modifications (a total of 20 major intermediate designs were considered and a total of 54 detailed models were constructed). Most of the design modifications were assessed based on the stress intensity level for level-5 torque input. Some modifications were rejected because of the excessive increase in weight that it produces or because of the difficulty in proposed fabrication procedures. The final design is shown in Figure 2.6 and an application for a US patent has been recently approved [11].

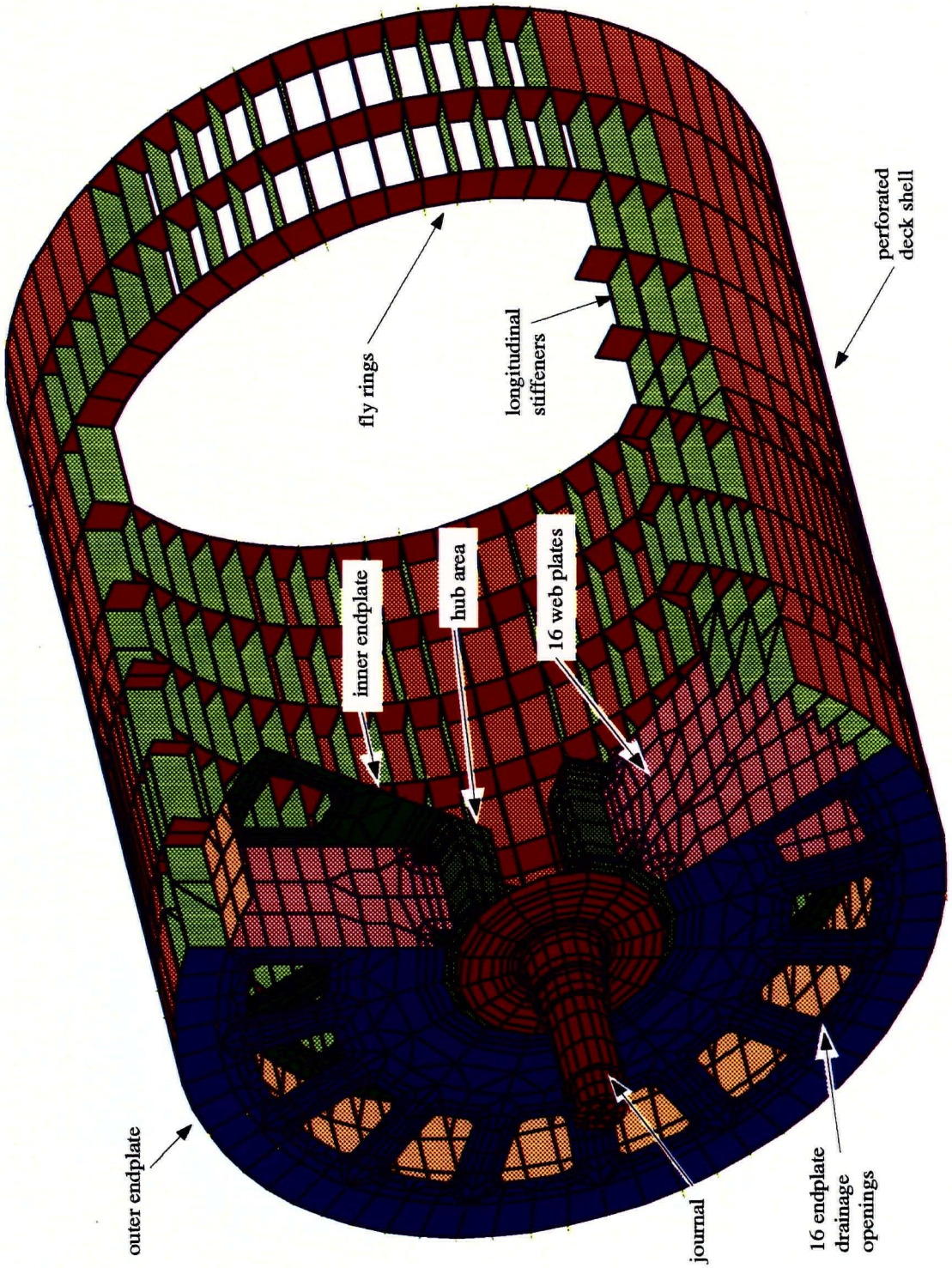

Figure 2.6: The new pressure washer drum design

After finalizing the concept of the new design, numerous size and dimensional variations were studied to arrive at the optimized shape and dimensions for the modified design. Among these were:

- Study the effect of end-plate and web-plate thickness including partial thickening of the plates.
- Study the effect of thickness variations in the cage or upper-deck structure.
- Study the effect of welding procedures and the number of welding points in the hub/end-plate area.
- Study the effect of changing the hub length and diameter. A special design optimization study was performed for this task.
- Study the effect of the number of web-plates in-between the end-plates forming the re-enforced sandwich structure.
- Study the effect of varying the length of the shrink fit area between the hub and the journal.
- Study the effect of varying the depth of the longitudinal member reinforcements and the circumferential fly ring reinforcements in the upper deck area.

Sample stress results for the original design and the proposed new design with summary of comparative stress intensities at various critical points are given in the following section.

2.2 FINITE ELEMENT ANALYSIS RESULTS

2.2.1 Results of the Original Design

The finite element analysis of the original drum model reveals the critical areas of stress to be located at the weld between the drive shaft and hub and the weld between the hub

and the spokes. Figure 2.1 shows the model used and Figure 2.7 shows some representative stress values obtained at the above locations for normal operating conditions. As seen from the figure, the FE analysis indicates approximately 68.95 MPa (10 ksi) von-Mises stress intensity at the weld between the drive shaft and the hub, and approximately 54.5 MPa (7.9 ksi) in the spoke weldment. Investigating the full stress picture for the weld area reveals that the stresses are almost all alternating at this location. It is believed that these alternating stresses, together with the welding residual stresses [12,13], estimated at approximately 207 MPa or 30 ksi, are the cause of the cracks evident after a short period of operation (approximately 2 years). A fractographic analysis of the failed weld in this area did not reveal any conclusive evidence of stress corrosion cracking problem and, therefore, fatigue is considered to be the major contributing factor to the failure of these drums.

2.2.2 Discussion of Proposed Design Modifications

The original drums are initially modified by cleaning and grinding the failed welds and then welding heavy plates over the hub area. These design upgrades are modeled and revealed only minimal improvement on stresses in the hub area. In addition, the study of these design modifications also shows that areas of the new welds, i.e. the added-on plates to the original structure, form new critical stress points. It is argued that better welding procedure as well as use of plug weld for the added-on plates may improve the stress picture and eliminate the problem. For this reason, a simulation of both fillet and plug weld conditions is carried out for the added-on plates. Plug weld conditions show relatively better stress picture but it was excluded because of the unacceptable stress levels, the intensive spread of residual stresses, and the more cumbersome practical welding procedure. It is

All stresses are unaveraged von-Mises stress in ksi.
Quoted stresses are the maximium of the shell element layers:
First values are for the drive end and the second are for the idle end.

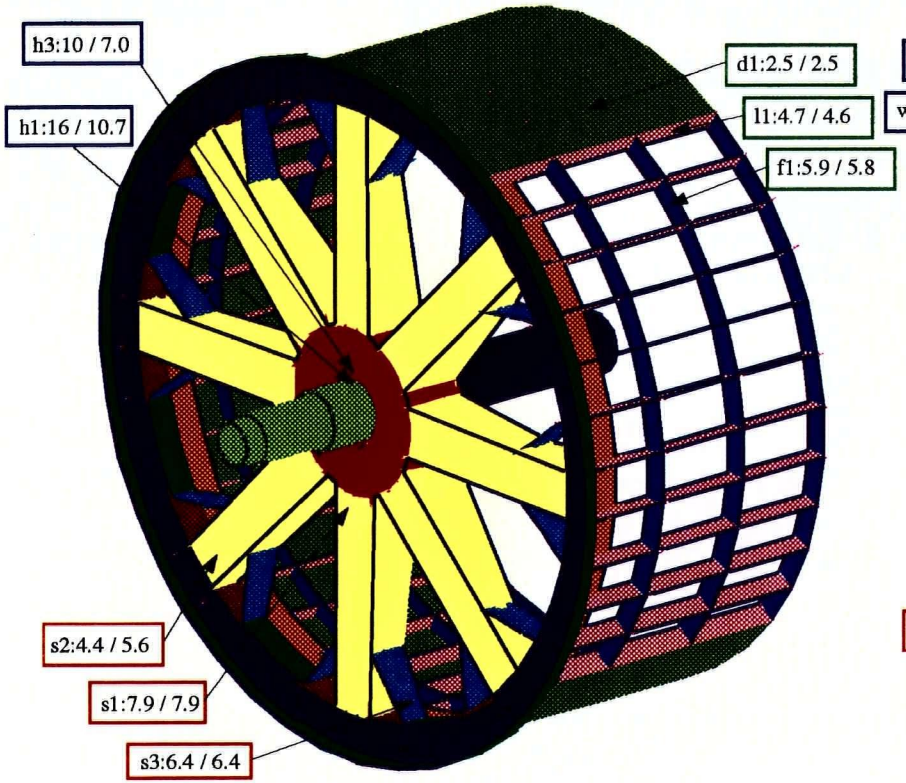

Figure 2.7: Stress results of the existing drum design

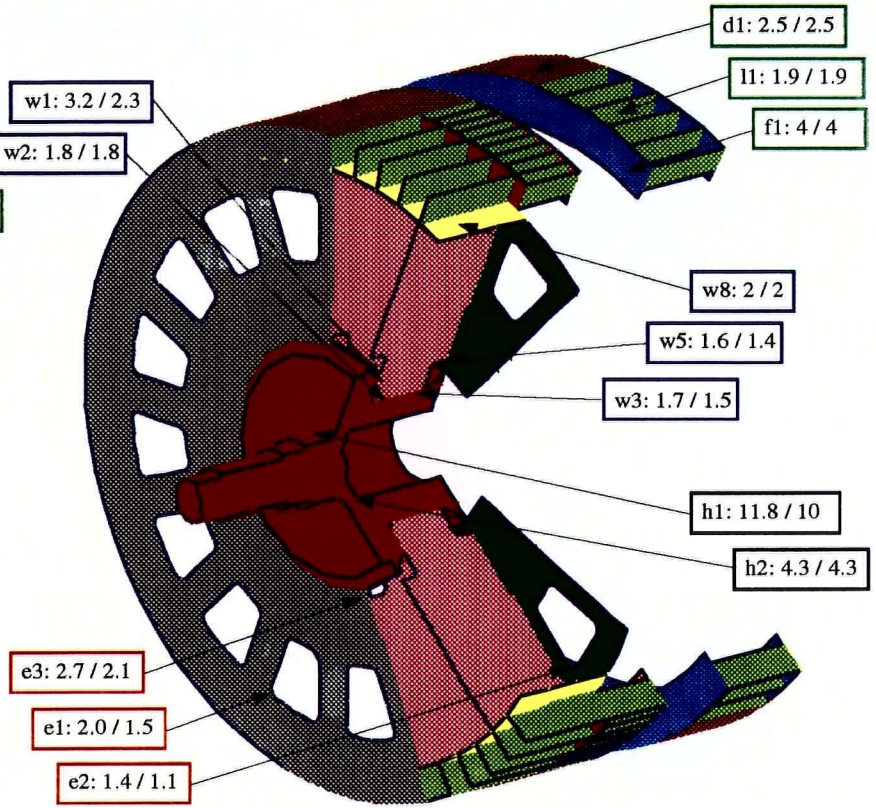

Figure 2.8: Stress results of the new drum design

concluded that reducing stresses in the hub area to an acceptable level requires a design modification that moves the weldments to a larger diameter. This leads to a design concept incorporating a large forged hub. This large hub is connected to the journal drive and provides a support to the internal pipe carrying the trough. This design concept gives better flexibility in choosing the hub diameter and allows for disassociation of functions between drum components.

It is also concluded that the use of spokes to transfer the load from the drive shaft to the deck is not desirable due to the stress concentrations created at the ends of the spokes. This is particularly evident at the spoke to hub intersection where extreme cracking occurred. This concept leads to the idea of modifying the design of the end components by using a continuous disc (end-plate) instead of spokes. After fine tuning and accounting for required hydraulic drainage, a double disc end-component design is developed (refer to Figure 2.5 and 2.6). The double disc design is formed as a sandwich structure with inner webs welded between the two discs or end-plates. This provides a much higher torsional and bending stiffness to both the drive and idle ends.

2.2.3 Results of the New Design

The new design results in a reduction of stresses of up to 70 % compared to the original design. The most critical area in the original design, the weld between the shaft and the hub at the drive end, has an alternating stress of approximately 68.95 MPa (10 ksi). The comparable location in the new design, the hub to end-plate weld, shows a maximum alternating stress level of only 18.62 MPa (2.7 ksi), see Figure 2.8 for details.

A comparison between stress levels for various critical points in the structure in the original and new design is given in Table 2.1. The finite element model values reported here are un-averaged von-Mises stress intensities.

Table 2.1: Comparison of stress results for original and new designs

EXISTING DESIGN			NEW DESIGN		
Location	Description	Stress* MPa (ksi)	Location	Description	Stress* MPa (ksi)
h1	shaft/hub intersection	110.3 (16)	h1	journal/flange intersection	81.4 (11.8)
h3	shaft shoulder/ hub plate weldment	68.9 (10)	e3	end-plate/hub weldment	18.6 (2.7)
s1	spoke/hub intersection	54.5 (7.9)	w1	end-plate/web-plate weldment	22.1 (3.2)
s2	spoke/box intersection	38.6 (5.6)	w8	web/box intersection	13.8 (2.0)
d1	deck shell	17.2 (2.5)	d1	deck shell	17.2 (2.5)
l1	longitudinal members	32.4 (4.7)	l1	longitudinal members	13.1 (1.9)
f1	fly-rings	40.7 (5.9)	f1	fly-rings	27.6 (4.0)

*Reported stresses are un-averaged von-Mises intensity for level 5 torque, 129 kN.m (1,141,000 lb.in.)

The alternating stress levels in the new design are less than 27.5 MPa (4 ksi) in the overall model with most of the structure experiencing an average alternating stress of 16.5 MPa (2.4 ksi). The relatively higher stress locations in the new design are at the drainage openings of the end-plates and the mouse hole openings on the stiffening webs between the end-plates. No refinement is made to the model for the larger drainage holes on the end plates. It is believed that proper rounding of the corners and grinding of the plasma burned

surface around the corners will eliminate any possible problem in this area. The second area, the mouse hole drainage openings on the webs between end-plates, is further refined. A variety of design alternatives including various mouse hole shapes and different radii dimensions are prepared. Each design alternative is modeled in order to arrive at the final optimized design shown in Figure 2.6.

Chapter 3

EXPERIMENTAL TESTING & STRESS RELIEVING

3.1 OBJECTIVES

The objectives of the conducted experiments [14] may be summarized in the following main points:

- Identify proper boundary conditions for the finite element model. This includes assessment of the pressure distribution in the forming board area and on the drum surface as well as an assessment of how the torque is transmitted through the outer deck and the central shaft.
- Provide sensitivity analysis for the pressure and friction force distribution on the drum surface.
- Verify critical stress locations on the drum.
- Assess the validity of the results obtained from the finite element model of the original and the modified design. This may be achieved by testing of an actual prototype of the drum under proper working conditions.

3.2 EXPERIMENTAL SETUP

Three separate experimental tests were conducted to achieve the above stated objectives.

3.2.1 Experiment #1: Assessment of Forming Board Pressure

Six sensors were installed on the back surface of the forming board area of a pressure washer at the Domtar mill in Redrock, Ontario (see Figure 3.1 for locations of the sensors). The pressure sensors were used to determine the exact pressure distribution on the drum face directly under the forming board in actual operating conditions. The obtained pressure values are used to fit a linear distribution for the forming board pressure and are then incorporated as boundary conditions in all finite element models.

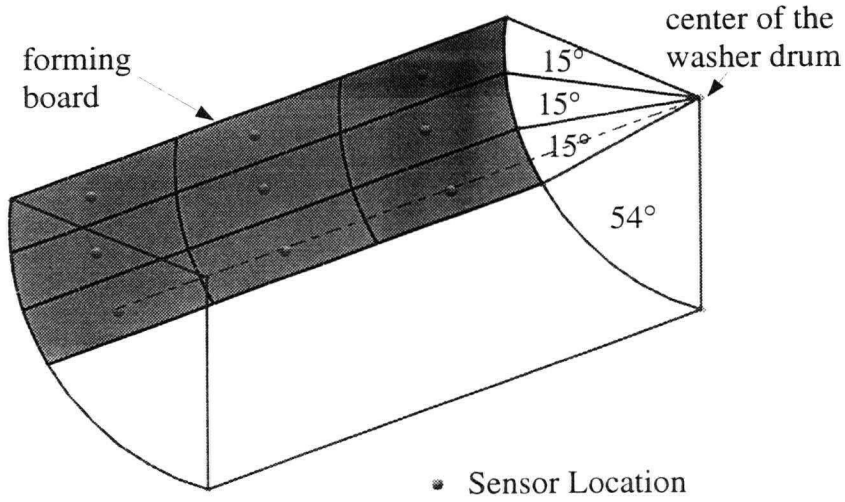

Figure 3.1: Sensor locations for experiment#1

3.2.2 Experiment #2: Assessment of Load and Reaction Distribution

A washer drum of the original design was acquired and transported to a testing ground in Thunder Bay, Ontario. This drum was used to study various friction distributions on the drum surface and its effect on the loading and the stresses in the spoke area, the transmitted torque through the central shaft and the stresses in the journal area. The frictional forces on the drum surface were simulated with circumferential cables with separate control on the tightening force of each cable. By changing the tightening force on the cables, the input

torque may be balanced or counteracted within a specified length of the drum surface, see Figure 3.2 and 3.3 for details.

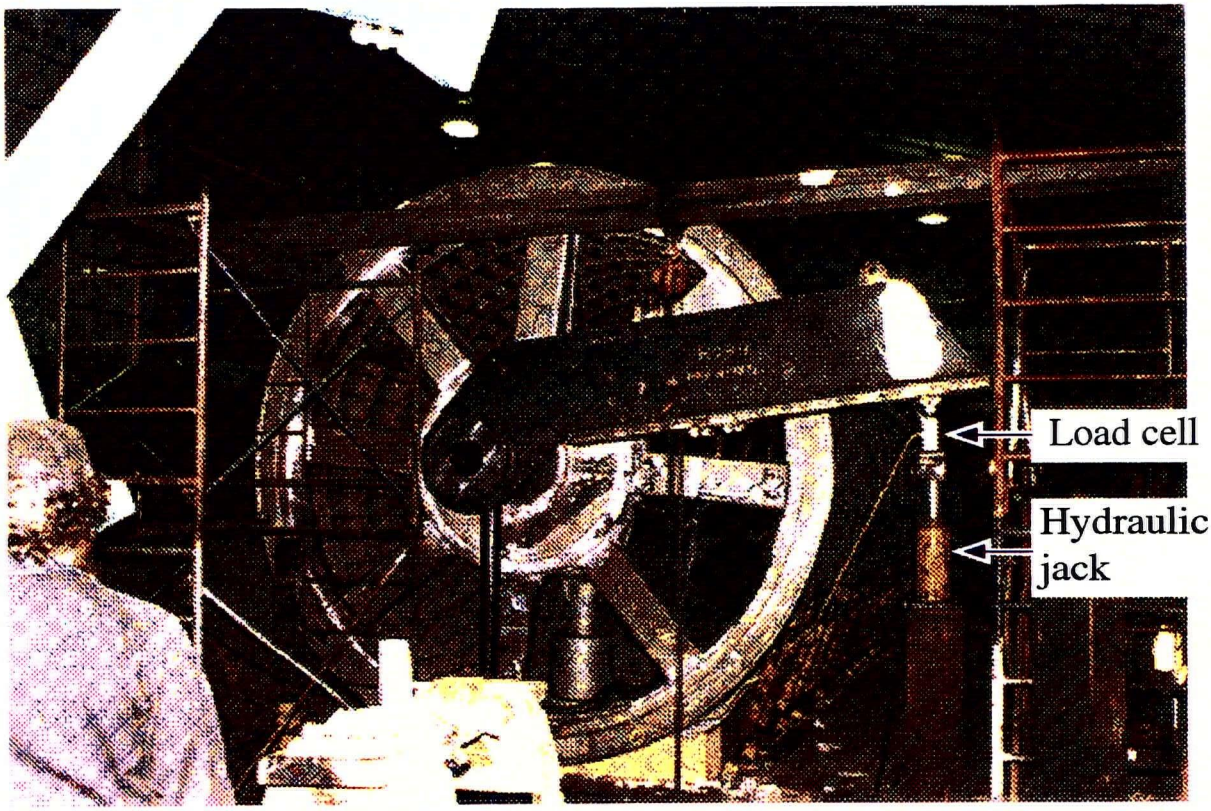

Figure 3.2: Setup for experiment-2

The input torque was applied through a heavy torque arm with an end force from a hydraulic jack. The experiment involved two load cases identified by different torque values and three separate cable support cases (i.e., by changing the tightening force along the drum axis) forming a total of six scenarios. These scenarios were repeated two times each to minimize possible experimental error.

Sensors were mainly mounted on the spokes while some were mounted on the central shaft next to the drive-end hub area (refer to Figure 3.4 for sensor locations) to measure the amount of torque transmitted through the shaft to the idle end. To measure the input torque

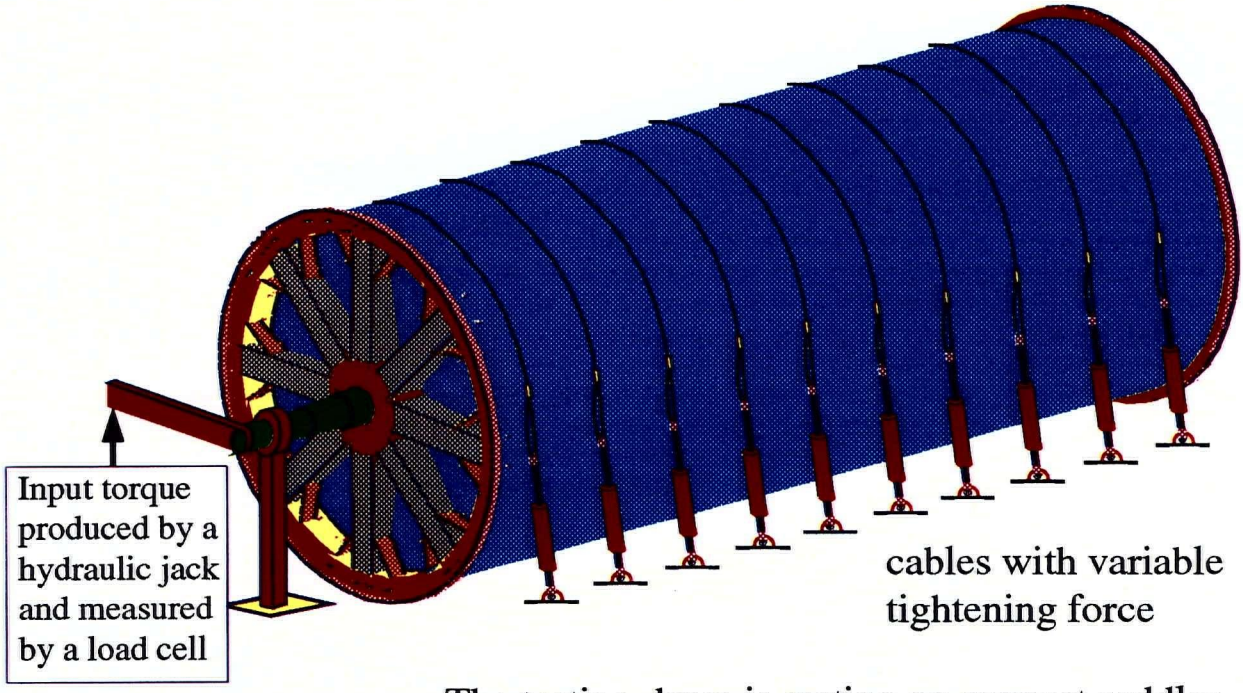

Figure 3.3: Torque application and cable setup for experiment-2

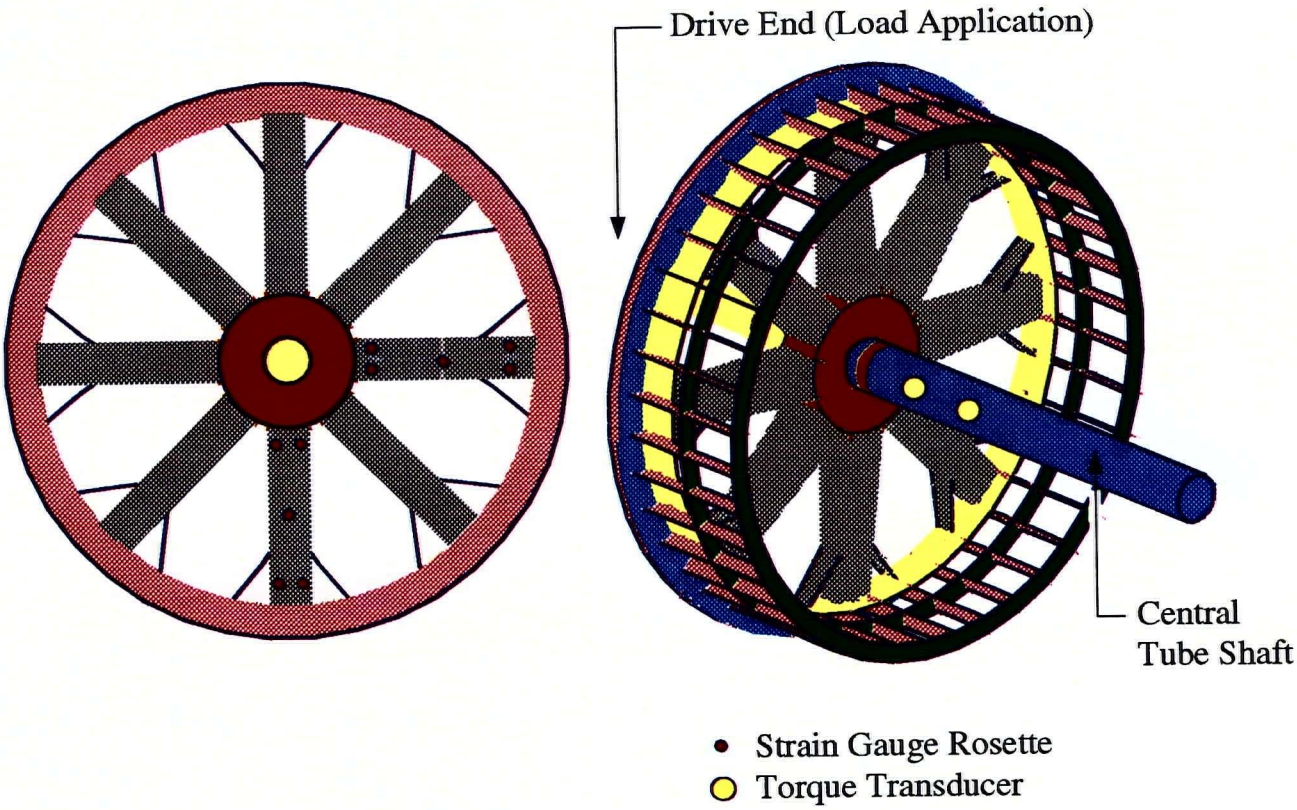

Figure 3.4: Sensor locations for experiment-2

accurately, a load cell was positioned between the hydraulic jack and the torque arm. The stresses and the torque were then calculated by measuring strains indicated by standard strain gauge rosette and one full bridge torque transducer. The torsional twist angle of the drum was measured by reference to a horizontally fixed wire along the axis of the drum.

3.2.3 Experiment #3: Assessment of Stress Results for the Final Design

To assess the finite element results of the final design, another set of experiments was performed on the prototype of the new design under actual operating conditions. The prototype is shown in Figure 3.5.

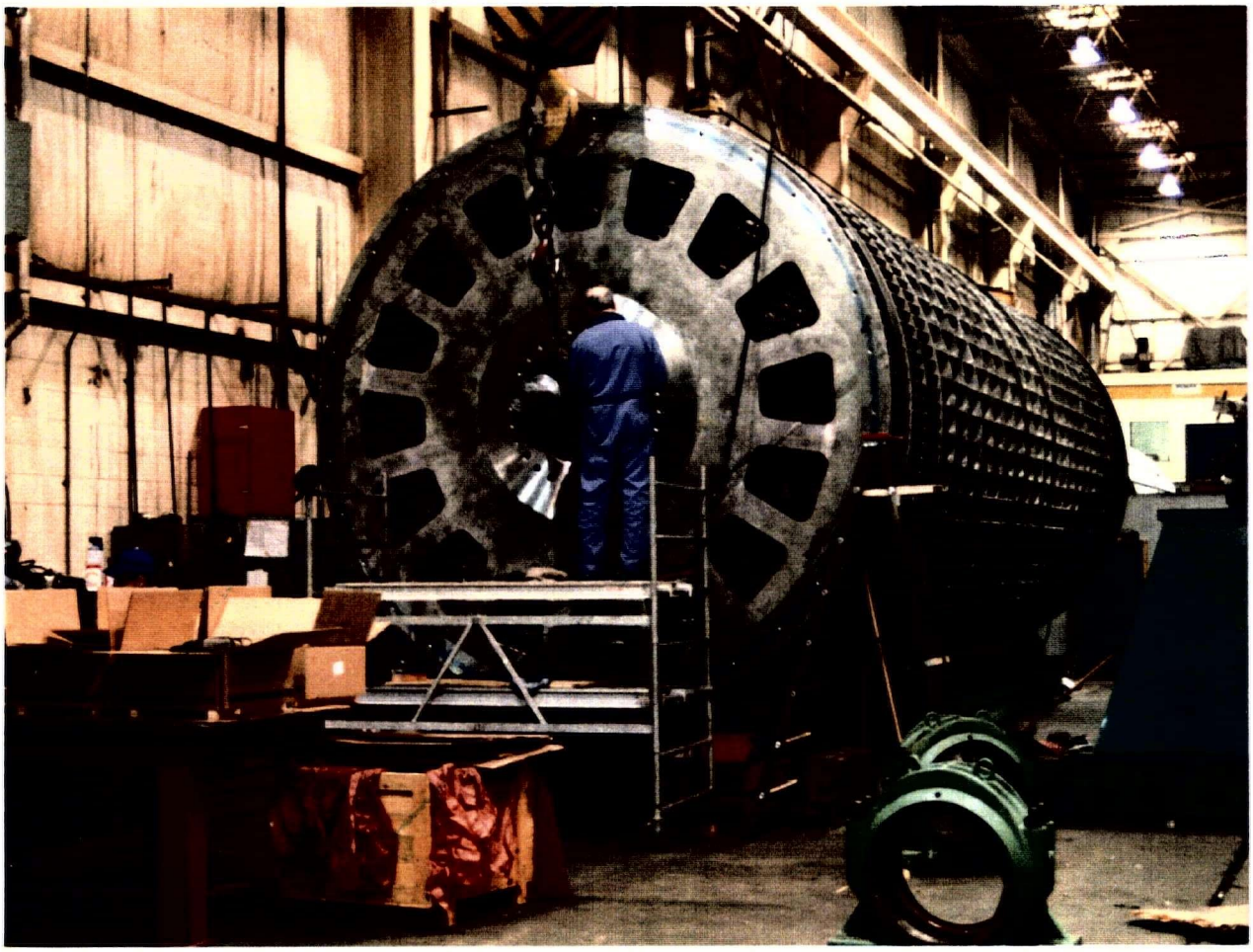

Figure 3.5: The prototype of the new proposed design

The new design was installed in one of Domtar mills in Red Rock, Ontario and it was equipped with special holes and passages to allow for wiring and sensors on various locations of the new design (see Figure 3.6). Sensor locations considered in the second part of this experiment were in the immediate area of the sandwich end-plate structure close to the journal weld and in the area of the inner shaft and the upper deck, see Figure 3.7 for details. Data from all sensors was recorded for the start-up conditions and for about 12 hours operating conditions after start-up. Two strain gauges were mounted on the mid-span deck surface of the actual prototype. Static strain was measured during the lifting of the drum and also when the drum was resting on support saddles.

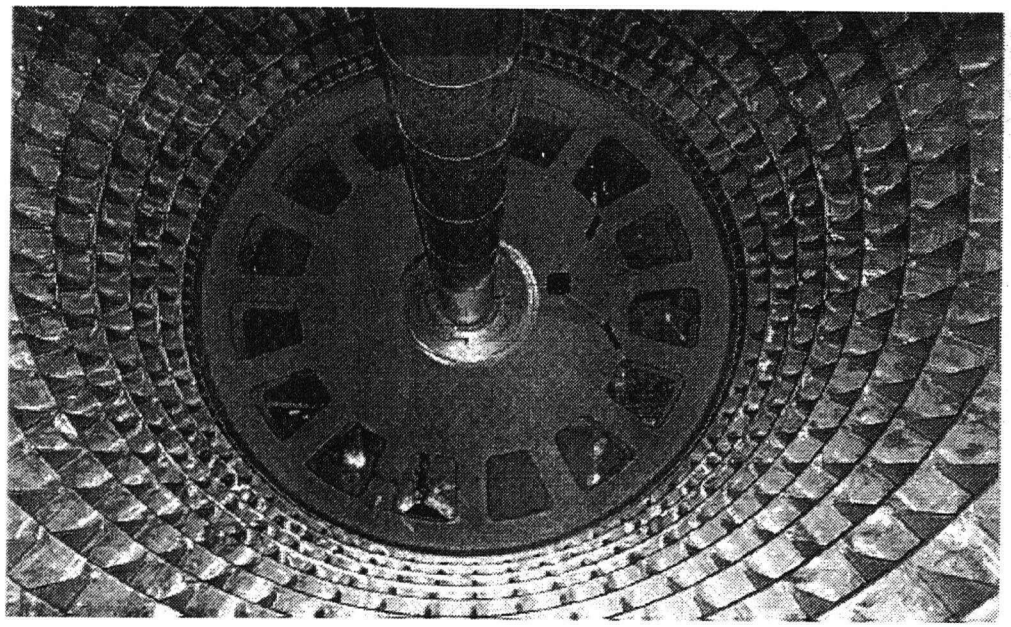

Figure 3.6: Setup of the sensor wiring for experiment-3

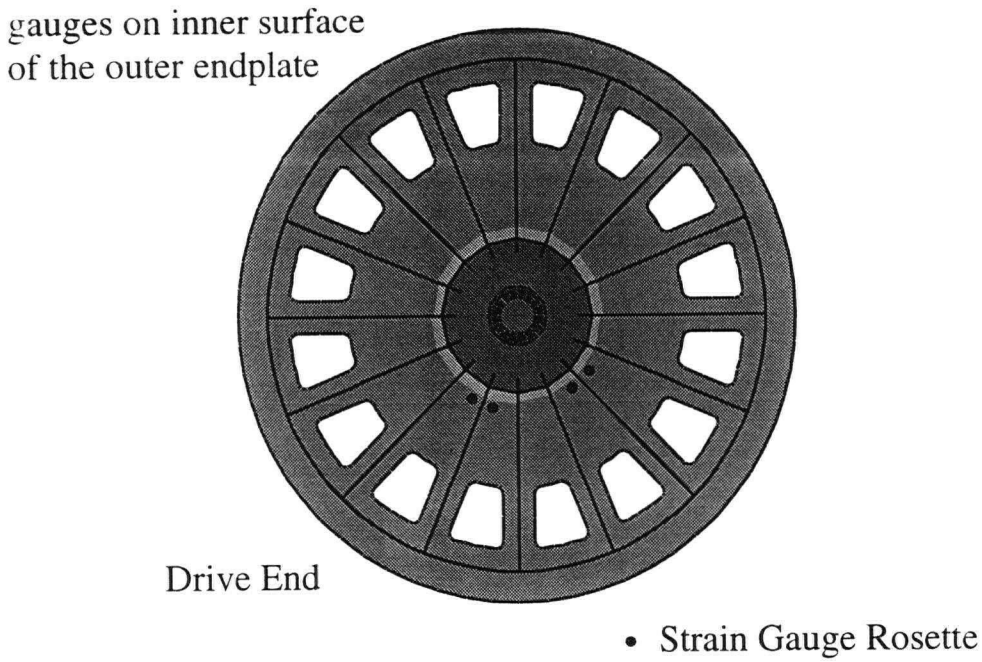

Figure 3.7: Sensor locations for experiment -3

3.3 EXPERIMENTAL RESULTS

3.3.1 Experiment #1: Assessment of Forming Board Pressure

As indicated above, six pressure sensors were installed on the surface of the forming board of one washer drum at the Domtar mill in Redrock, Ontario. A special arrangement was designed to prevent blocking or clogging of the tubes leading to the sensor location. A separately controlled line of air pressure was fed to the end of the tubes allowing the pulp to partially extrude out and be sustained by the air pressure.

The measured pressure values reveal very little variation of pressure along the drum face in the axial direction. Linear variation of pressure along the height of the drum was assumed. The recorded pressure values under these assumptions showed a value of 13.8 kPa 2.0 psi) at the top and a maximum value of 44.8 kPa (6.5 psi) at the bottom of the forming board. A design value of 55.2 kPa (8.0 psi) for the bottom with a linear reduction to 13.8

kPa (2.0 psi) at the top of the forming board was used for all numerical models. Finite element sensitivity runs (results of various sensitivity tests are shown in Figure 3.8) indicated that the resulting stress levels in the drum were highly dependent on the pressure in the forming board area.

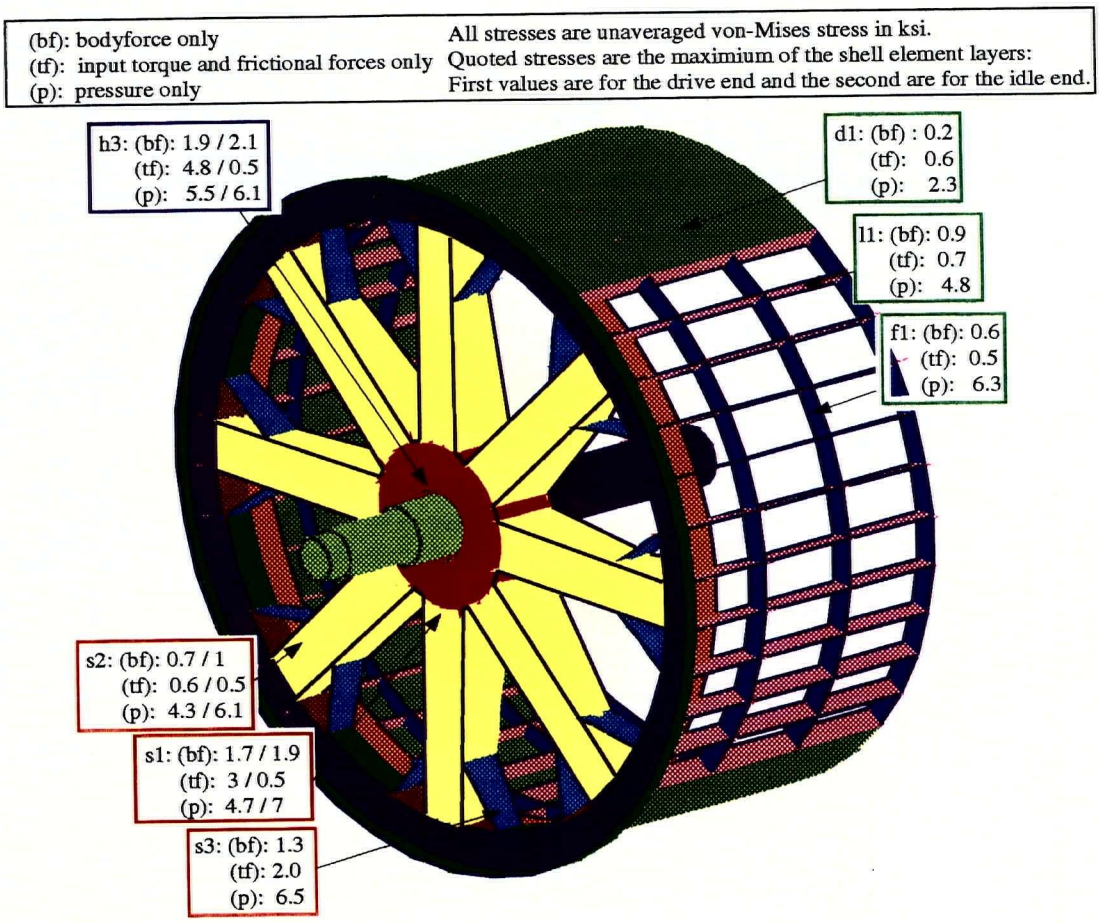

Figure 3.8: Stress results of the sensitivity runs

3.3.2 Experiment #2: Assessment of The Load Distribution

The pressure and frictional forces on the drum surface were simulated with circumferential cables each with a separate tensioning adjustment. Data obtained from the torque sensors indicated that no significant amount of torque was transmitted to the idle end through the central shaft and the drive end [15]. This important conclusion led to the idea of

separating the central shaft or possibly eliminating it entirely. Depending on the process requirement for having a liquor trough, the central shaft may be eliminated entirely. An experiment was performed at Domtar to measure the washing efficiency with no trough. The experiment indicated that two stage washing using the liquor trough had no process advantage over single stage washing. It is therefore, advisable to eliminate the liquor trough and the central shaft.

The data obtained from the strain gauges (located at the spokes) indicated that the spoke/hub area is the most critical area of concern in terms of stress level. This agrees well with the numerical results obtained from the FE simulations.

3.3.3 Experiment #3: Assessment of Stress Results

To assess the finite element model results, another set of experiments was performed on a prototype that was built by Tristar industries in Delta, British Columbia, Canada and installed at Domtar mill in Red Rock, Ontario. The data collected from the hub area sensors indicated stress levels very close to the finite element model results (refer to Table 2.1 for FE results). The area of the end-plate near the hub weldment measured a stress of 17.9 MPa (2.6 ksi) which compares very well with the model results of 18.6 MPa (2.7 ksi) in the same area [16].

3.4 STRESS RELIEVING

3.4.1 Heat Treatment of Austenetic Steels

To reduce the risk of fatigue cracking and in an effort to eliminate or reduce welding induced residual stresses, the critical hub to end-plate weld is fully X-rayed and the entire end component is thermally stress relieved. Austenetic steels should generally be heated to about

900 °C (1650 °F) to attain adequate stress relief. In some instances, heating to the annealing temperature may be required. Holding at a temperature lower than 870 °C (1600 °F) will result in only partial stress relief. Sometimes austenetic steels are stress relieved at temperatures normally used for carbon steel, i.e. 540 to 650 °C (approx. 1000 to 1200 °F). It should be noted that, although at these temperatures virtually all residual stresses are relieved in carbon steels, only 30-40% of residual stresses are relieved in austenetic steels [12,13].

Heating to the higher level temperatures may have adverse effects on the mechanical and corrosion properties of austenetic steels. Among the important characteristics to be considered, is the precipitation of intergranular carbides and the formation of sigma phase. The low carbon content of the 316L type austenetic steel (normally 0.03% max.) reduces precipitation of intergranular carbides to safe levels. Thus, this steel may be held at the sensitizing range of 430 to 815 °C (approx. 800-1500 °F) for periods of up to 2 hours and cooled slowly without experiencing dangerous levels of intergranular carbide precipitation [17-20]. On the other hand, because 316L contains molybdenum, it will be susceptible to the formation of the hard brittle sigma phase when sensitized at this temperature. Furthermore, the composition of most austenetic stainless welds is intentionally adjusted so that ferrite will be present as a deterrent to cracking. This ferrite may transform to sigma during the stress relieving process [16-20]. The presence of sigma phase can deteriorate both corrosion resistance and ductility of the steel. It is shown, however, that corrosion resistance of the 316L type may be significantly improved by holding at 885 °C (1625 °F) prior to stress relieving at 675 °C (1250 °F) [18,19]. Also heating to a level of 815 to 925 °C (1500-1700 °F) will cause the coalescence of chromium carbide precipitates or the formation of sigma phase to a form less harmful to corrosion resistance and mechanical properties of the 316L

type steel.

3.4.2 Stress Relieving Process

From the above considerations, a heat treatment process is chosen. It is decided to heat the end component of the drum to a temperature of 925 °C (1700 °F), hold for 3 hours, control furnace cool at a rate so that the temperature difference is not more than 65 °C (150 °F) between the thickest and thinnest part until 425 °C (approx. 800 °F) is reached. At this point the parts and weldment will be allowed to slowly cool down within the furnace. It is believed that this process will eliminate about 70-85% of the residual stresses in the steel [18,19]. This may bring the residual welding stress from approximately 200 MPa (30 ksi) to 30-60 MPa (5-10 ksi). Specially designed electric furnace, to accommodate the drum component, is used and air is considered to be satisfactory furnace atmosphere. Crack growth rate tests were performed on test specimens taken after stress relieving and the results indicated that the weldments were not adversely affected by stress relieving.

Chapter 4

SHAPE OPTIMIZATION USING FINITE ELEMENTS

4.1 BACKGROUND

In the new design discussed in chapters 2 and 3, the hub is the heaviest single part in the structure. Forging of such heavy part is expensive and may require special equipment and attention. To optimize this part of the structure, a three dimensional shape optimization analysis is performed using the SHAPE finite element optimization package [21].

A generalized mathematical form of a design optimization problem may be described in the following equations:

It is generally required to find an n-design variables in a design vector $x = [x_1, x_2, x_3, ...x_n]^T$, to minimize a cost function:

$$f(x) = \textit{volume or mass or weight of the structure,} \tag{4.1}$$

and satisfies the state equations:

$$[K(x)]\{u\} = \{P\}, \quad u = 1,r \ \textit{(i.e., r state variables)} \tag{4.2}$$

and the inequality constraints

$$g_j(x,u) \leq 0, \qquad j = 1, m \ \textit{(i.e., m inequality constraints)} \tag{4.3}$$

The constraints may be placed on displacement limits, stress limits or natural frequency limits. In the case of natural frequency constraints, the state equation should represent the dynamic behavior of the structure. The set of inequality constraints includes, as a subset, physical upper and lower bound limits on the design variables.

Each constrained response r_i can be represented in terms of the element contributions by:

$$r_i = \sum_{j=1}^{n} \frac{c_{ij}}{v_j} \tag{4.4}$$

where n is the number of elements in the model, v_j are the element volumes, which are the implicit design variables, and c_{ij} is some form of element contribution to the response quantity. In the same way, the total material volume of the structure may be given by

$$V = \sum_{j=1}^{n} v_j \tag{4.5}$$

In the case of simple variable limit constraints, the constraint equations may be written in the following normalized form:

$$(r_i / r_i^*) - 1 \leq 0 \ , \quad i = 1,...,m \tag{4.6}$$

where r_i^* is a normalizing quantity for the response variable r_i. The optimization program, then, uses the Lagrange multiplier method to generate what are generally known as the optimality criteria expressions given by the Lagrangian function:

$$L = V + \lambda^T \bullet f \tag{4.7}$$

where

$$f_i = \left(\frac{1}{r_i^*} \sum_{j=1}^{n} \frac{c_{ij}}{v_j} - 1 \right) \tag{4.8}$$

and λ_i is a Lagrange multiplier associated with the ith constraint. The optimality criteria expressions are then obtained by setting

$$\left(\frac{\partial L}{\partial \tilde{v}} \right) = \tilde{0} \tag{4.9}$$

where $\tilde{0}$ is a zero vector.

The next stage involves a series of intermediate iterations or designs aiming at increasing the efficiency of the design and trying to insure the satisfaction of the constraints. In the shape optimization program used in this analysis, the measure of efficiency of a particular design is the "virtual volume" obtained as the ratio of the material volume to the most critical factor (limiting value of response/actual value of response) to the constraint surface. At this stage, some of the previously removed elements may be restored to the structure based on the results of sensitivity analysis.

This iterative intermediate design stage ends when the program selects one of the generated designs as the most efficient design. This completes one "design step". The next design step is a repetition of the outlined procedure, starting with this most efficient design from the last design step. The optimization process will continue until the user specified total number of iterations or design steps is satisfied. Execution will end earlier if the program is unable to improve upon the last most efficient design generated.

4.2 THE HUB SUB-MODEL

The following stages are performed in the modeling and the design optimization of the hub:

- For the final accepted design, perform a finite element analysis with the design loading conditions and extract detailed results around the boundary of the area to be optimized, i.e., the hub boundary.
- Build a more detailed finite element model for the part to be optimized. The number of elements in this model may be one order of magnitude larger than the number of elements

– Impose field solutions of the original model as boundary conditions for the detailed model.

– Perform a finite element design optimization analysis to find the optimum shape.

Approximately 30,000 elements and 48,000 DOF are used in the sub-model of the drive-end hub area. The sub-model contains details of the solid hub and part of the journal as well as parts of the end-plates and web-plates that allow specifying the boundary conditions. All elements except those on the hub surface are 'frozen' so that the optimization process will only remove elements from the surface of the hub. Input torque and reaction forces of the motor are applied to the end of the drive-end shaft while the displacement solution of the full model are used as displacement constraint along the boundary of the sub-model.

The sub-model is built with an over-design and uniform thickness hub size and the total material volume is to be minimized. The model is then submitted to the shape optimization software and a smoothed optimized contour of the hub surface is determined.

4.3 OPTIMIZATION RESULTS

The full optimization run took more than 100 iterations and approximately 34 hours of CPU time on a Hewlett Packard Apollo 735 workstation. As shown in Figure 4.1, the optimization process starts with an over-sized 22 cm (8.7 in.) thick hub with outer diameter of 81.3 cm (32 in). A maximum stress level of 20.6 MPa (3 ksi) is specified as a user constraint. Attention has been given to the stress level along the shaft to flange connection, shrink fit area, web/ end-plate weldment, and the weldment between the webs and the hub. The analysis reveals the following conclusions:

– The stress level along the web to flange weldment (labeled as w1 in Figure 4.1) is the most sensitive affecting the hub size reduction.

– The continuing curved surface at the ends of the hub area contributes to lowering the stress near the hub and inner end-plate weldment.

A longer weld between web-plates and hub will reduce the stress level around the mouse hole drainage openings.

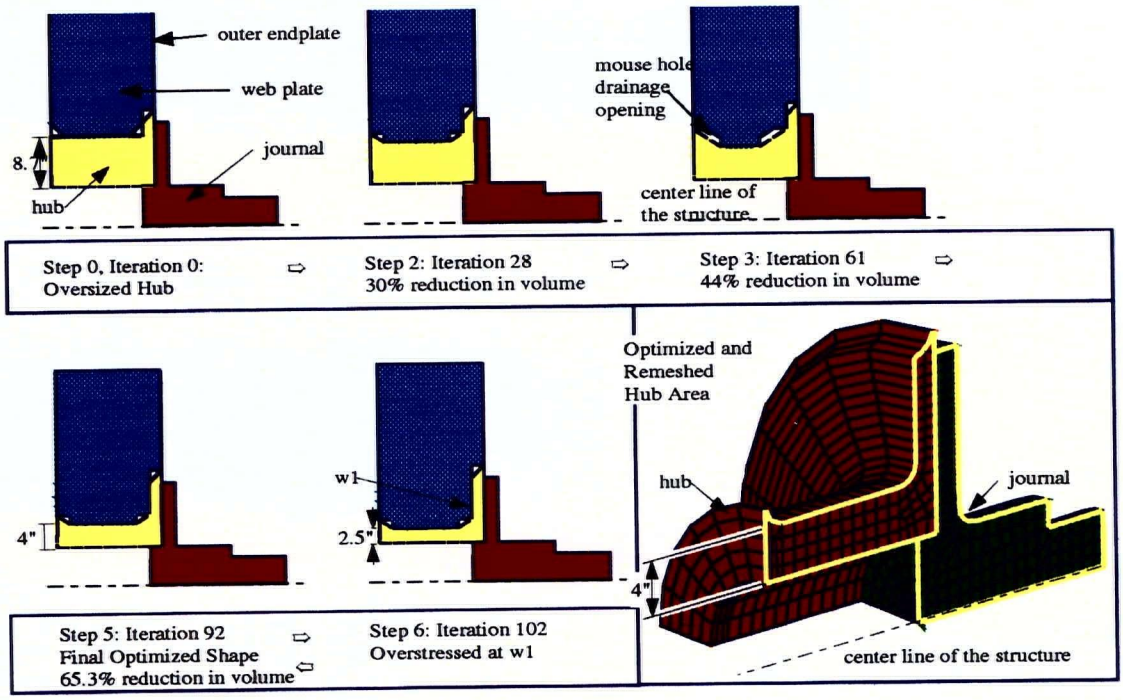

Figure 4.1: Optimization of the new solid hub

Although a washer drum is geometrically axisymmetric, the loading and boundary conditions are not. This is expected to lead to an optimized hub that is not axisymmetric since the analysis performed is simple static analysis. After the optimization process is completed, the new hub model is made axisymmetric by the user. This newly constructed hub model must adapt to the most conservative section profile along the circumference of the optimized model.

The final result presents a new drive end and hub assembly with an optimized surface profile. The curvatures and smoothness of the surface have to be handled manually. The

new hub design is 10.2 cm (4 in.) thick at mid-span (55.9 cm or 22 in. outer diameter) with continuing curved surface at the ends. It contains 65% less material than the original over-designed model and the stress level in the entire hub assembly is more uniform with a maximum critical stress value of 20 MPa (2.9 ksi) at the webs to hub weldment (refer to w1 in Figure 4.1). Results of selected intermediate and of the final iterations from the optimization program are also given in Figure 4.1.

Chapter 5

FATIGUE LIFE PREDICTION OF THE NEW DRUM DESIGN

5.1 INTRODUCTION

Pre-existing defects, internal flaws or surface cracks are common in structural components specially with welded joints and they may develop into larger cracks under the influence of regular service loading and, finally, lead to component failure. The short service life of the existing drum design has shown the significance of such failure mode. Accurate calculations of the stress intensity factors (SIF) of these cracks are thus essential for reliable prediction of the crack growth rate and the fatigue life of the component.

With the development of isoparametric and singular elements [22-24], the finite element method (FEM) has been considered one of the most powerful numerical techniques for the solution of linear elastic fracture mechanics (LEFM) problems. The finite element solutions have also been shown to be very effective in crack propagation as well as fatigue life prediction problems [25,26]. The method has great potential in solving complicated three dimensional problems as well as in solving nonlinear fracture mechanics applications. In order to efficiently apply the FEM to such problems, however, certain important steps and preparations have to be considered. Among these are the tedious and time consuming step of preparing a detailed three dimensional mesh for the structure, the implementation of the singular element in the mesh and the post processing of the data. For the foregoing reasons, commercial finite element programs and fatigue and fracture programs have developed an approximate method for the analysis of such problems. In this method, a pre-existing crack

with well defined shape is introduced in a simple structure. Available crack shapes may be chosen from standard ones such as penny-shaped, elliptical, thumb-nail, etc. The component geometry is generally simplified to be an infinite plate, a thick or thin-walled cylinder in two or three-dimensional situation. Loading may be a single type, e.g., simple tension, bending, shear or torsion, or a combination of such loadings. The user is then asked to choose combination of these 'canned' features that will best represent the behavior of the actual structure. Most of the available features do have existing analytical results and may be easily programmed to calculate various fracture mechanics parameters and fatigue life predictions. It is believed that this kind of analysis and approximation may in certain cases produce inaccurate results and the life predictions produced through this analysis may be non-conservative.

5.2 OBJECTIVES

The objective of this chapter is to test the accuracy of the above standard method against a more detailed numerical procedure [27]. The calculation of fracture parameters, e.g., SIF versus crack length curve, through establishing a detailed finite element sub-model for the critical part of the structure under real life loading conditions is proposed. For the detailed FE sub-model, the stress intensity factors (SIF) will be calculated for various crack lengths introduced in the actual geometry using displacement extrapolation methods. The fatigue life cycle of the structure will then be estimated based on the calculated SIF and Paris Law.

In the remaining part of this chapter, we start with a brief overview of the conventional and singular element analysis for fracture mechanics problems, introduce the

sub-modeling procedure and analysis and, finally, compare results of the two methods and provide some conclusions.

5.3 ELASTIC SINGULAR ELEMENTS

5.3.1 Crack Tip Stress Field

For the general crack front in a three-dimensional solid shown in Figure 5.1, the stress field surrounding the region has the form [28]:

$$\sigma_{ij} = \frac{1}{\sqrt{r}}(f_{ij}K_{I} + g_{ij}K_{II} + h_{ij}K_{III}) \tag{5.1}$$

where K_I, K_{II}, K_{III} are the stress intensity factors associated with the three modes of fracture, and f_{ij}, g_{ij}, h_{ij} are angle dependent expressions related to the geometry of the structure.

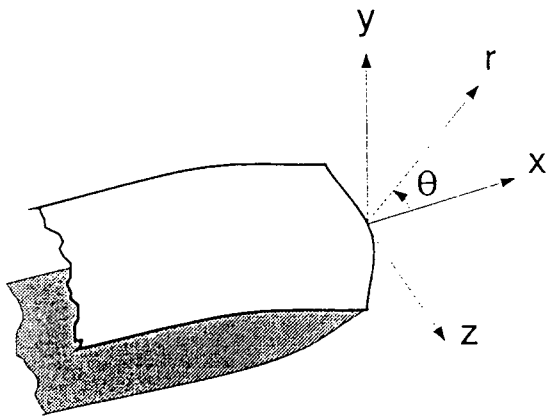

Figure 5.1: Three-dimensional crack front

From the above equation, the stress field becomes infinite as r approaches zero ($\frac{1}{\sqrt{r}}$ singularity) and so to obtain accurate values of the stress field or stress intensity factors, the square root singularity must be taken into consideration. Various approaches to the finite element modeling of cracked elastostatic bodies have been presented in the past. Only the conventional and singular finite element ones will be covered and considered in this section.

5.3.2 Modeling with Conventional Finite Elements

In this method, extremely fine mesh of standard or conventional elements is used to accurately model the deformation and the stress field in the vicinity of the crack tip. In two-dimensions, early work [29] produced reasonable accuracy for simple Mode-I problems with conventional linear and quadratic elements. In three-dimensions, application of 20-node isoparametric elements near a crack front may yield reasonable solutions with reasonable meshes but it may be difficult to obtain higher levels of accuracy with this element or with the linear conventional elements.

The development of higher order elements such as higher order isoparametric family of elements in P-version programs makes it feasible to produce more accurate results with a relatively coarse mesh. An extension to the use of conventional elements involved the use of sub-structuring technique or what is normally called super-elements. In this approach, the global structure is subdivided into several sub-structures with a coarse mesh. The area near the crack is then remodeled as a 'super-element' using a very fine mesh density. As first introduced [30], this technique produced reasonable results without undue computational requirements. The major advantage is the ability to handle complex geometry without time consuming mesh and CPU requirements. The method suffers, however, the shortcomings of having to perform three different analyses and to manage the file transfer between them and it is also mostly linked to the use of conventional elements.

5.3.3 Modeling with Early Singularity Element

In 1969, Wilson [31] presented the first method which directly addressed the square root singularity. His approach (strictly two dimensional) identifies a core region surrounding the crack in which the displacement field is known (except the stress intensity factors). The

remainder of the domain is modeled using conventional finite elements. The finite element formulation is modified to include minimization with respect to the unknown stress intensity factors in addition to the nodal degrees of freedom. The result is a system of linear equations which predict the nodal displacements and the stress intensity factors directly. It was the first finite element formulation which addressed the crack tip singularity in a valid and consistent manner.

Recognizing the limitations and problems of the core region method, several authors have proposed incorporating the asymptotic nature of the strain (or displacement) field directly into the shape functions of the element. Tracy [32] employed a simple polynomial displacement field within a triangular element. This approach was subsequently generalized to a family of elements. These elements use shape function formulations which produce the correct strain singularity. The primary unknowns, however, are the nodal displacements. The stress intensity factors must be calculated through post-processing.

5.3.4 Modeling with the Quarter-Point Elements

Henshell and Shaw [33], in 1975 and Barsoum [24], in 1976, noticed that by displacing the mid-side node in an eight-node quadrilateral element to the quarter-point position, as shown in Figure 5.2, the element strain field naturally exhibits an inverse of square root singularity. Hanshell and Shaw [33] tested their element against the undistorted element and compared the two results obtained with some known accurate solutions. In these tests, the values of the stress intensity factor K_I were obtained using the displacement extrapolation method. The quarter point element solution were more accurate in all of the tested cases.

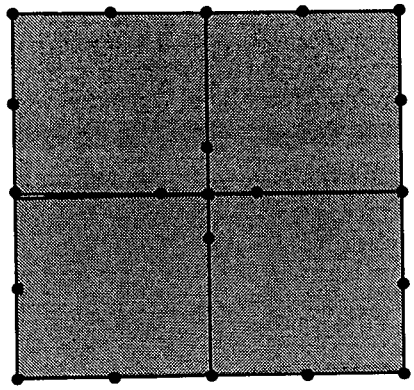

Figure 5.2: Rectangular elements with mid-side nodes at the quarter point

One important advantage of the quarter-point elements is that they can be used with any finite element code which has an 8-node quadrilateral element for two-dimensional analysis or a 20-node brick element for three-dimensional analysis. In the geometry definition, the user can displace the mid-side node to form singular quadrilateral elements as required and the square root singularity is produced automatically. The problem with these elements lies mainly in the special attention required for post processing of the results.

5.4 THE FINITE ELEMENT SUB-MODELING PROCEDURES

5.4.1 The Sub-Model

Various sub-models consisted of 3D 8-node quadrilateral shell and 20-node hexahedron elements of the drive-end of the new pressure washer drum are created with locally refined mesh as shown in Figure 5.3. Coarse mesh is used for the area away from the crack. The major advantage of such sub-modeling technique is the ability to reduce the total DOF of the model and thus reduce the CPU time and disk space required.

The sub-model is basically a cut-out of the drive-end structure from the global FE model in a way that the nodal points along the boundary of the sub-model will coincide, in

terms of nodal coordinates, with those in the full model. It is necessary to do so since the displacement response of the global model, which is analyzed with the full set of boundary conditions, will be used as prescribed displacements along the boundary of the sub-model. This also eliminates the need for any interpolation along the boundary that may introduce some approximation in the overall behavior of the sub-model. In essence, the sub-model actually behaves as a superelement. Therefore, the field solutions of the sub-model, with the prescribed displacements as boundary conditions, will be consistent with those of the global model under complete set of real-life boundary conditions.

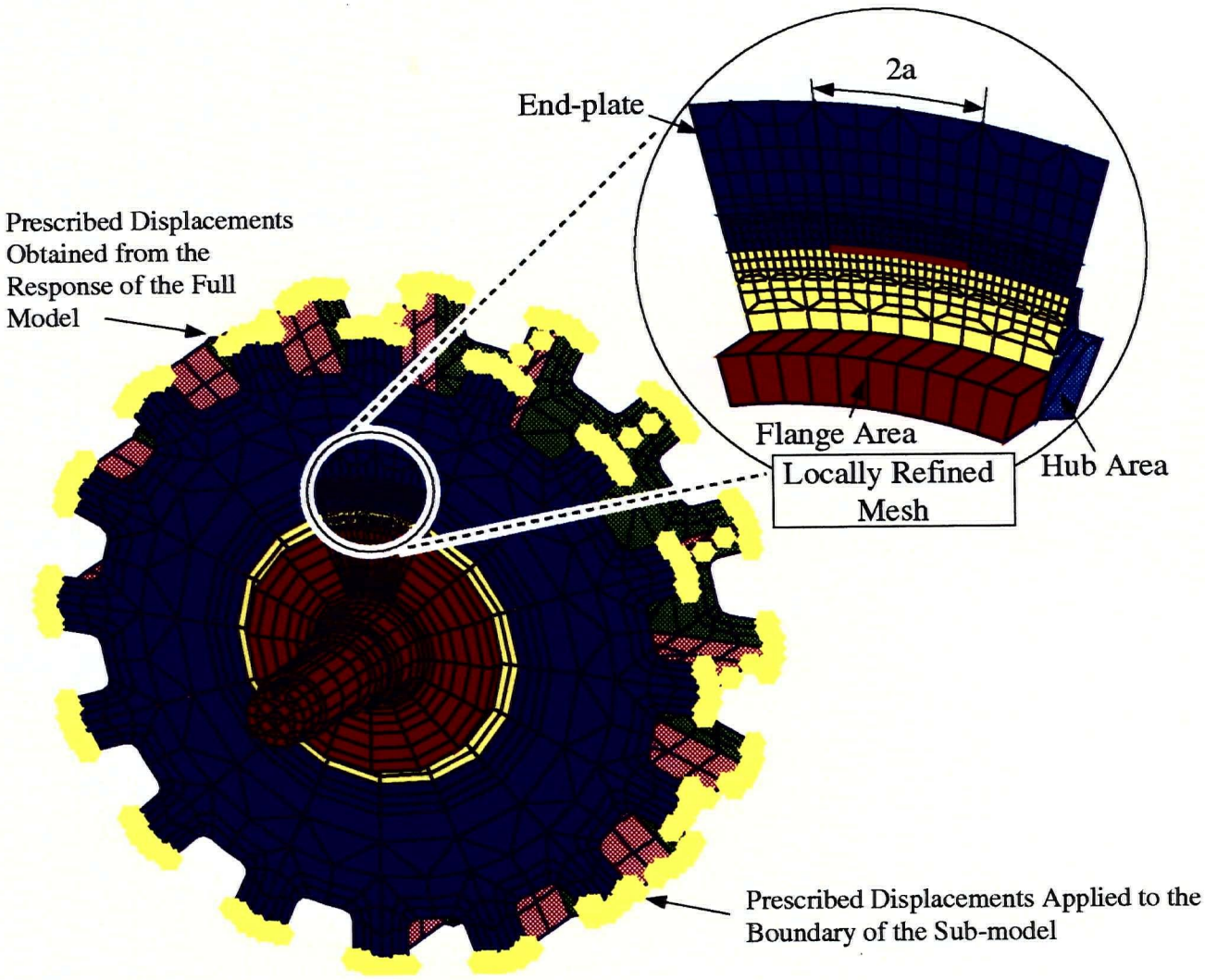

Figure 5.3: The sub-model used for the fatigue life prediction

The constructed sub-model contains approximately 46,000 degree of freedom (DOF). The sub-model is mainly comprised of the following components of the washer drum:

- The end-plate sandwich structure with 16 web-plates in between, up to the end-plate drainage openings.
- The solid hub/ flange combination (journal).

The refined mesh is mainly localized at the intersection of the hub and outer end-plate, where a rapid change of thickness of material as well as a weldment take place. This area is chosen based on the results of FE simulations for the full model which indicated that this area is the most critical one in the drum structure. Due to the complexity of the geometry, various element shapes, including 3D hexahedron, wedge, tetrahedron, pyramid solid elements, quadrilateral and triangular 3D shell elements are used. Close attention is given to the element qualities, in terms of aspect ratio and element distortion factors, to avoid poor accuracy caused by distorted element.

5.4.2 The Boundary Conditions

Since the nodal points along the boundary of the sub-model are coincident with those in the global model in terms of nodal coordinates, the nodal displacement solution from the global model, under the boundary conditions specified in Chapter 2, can be directly used as prescribed displacements (6-DOF per node) for the nodes of the sub-model. Test runs have shown that the stress and displacement responses of the sub-model are consistent with those of the full model. Boundary conditions applied to the sub-model are summarized as follow:

- Prescribed displacements from the displacement response of the full model.

– Input torque and reaction forces applied to the end of the drive-shaft.

5.4.3 Modeling of the Crack

Nodal points along the intended crack surface are 'unmerged' to allow the simulated crack to open when loading is applied. Three dimensional 8-node quadrilateral shell and 20-node hexahedron elements are used and the nodes which are in the vicinity of the crack tip have been shifted by a quarter edge length toward the crack tip in order to create the quarter-point elements to model the near crack tip singular strain field. Since the actual washer drum is rotating inside the washer housing (vat), the SIF will be varying for different angles about the axis of revolution. The simulated cracks are, therefore, located at 0°, 90°, 270° and 360° along the hub circumference. This necessitated building and processing four different sub-models for each increment of crack length. The crack length, starting from 0.59" is then extended along the circumference of the end-plate-hub interface area incrementally to 1.76 inch. A total of 4 models and 20 cases are constructed and processed. The idea of having one sub-model with four different cracks at the given angles is not viable for two reasons; first the size of the sub-model will be extremely large and second to avoid any possibility of remote interaction between the cracks.

5.4.4 Evaluation of the Stress Intensity Factors (SIF)

Once the FE field solution is obtained, there are essentially two approaches to calculate the stress intensity factors (SIF); the displacement field approach [29] , and the nodal force approach [34]. These approaches are based on the asymptotic displacement field and stress

field near the crack tip, given by:

$$\sigma_{ij} = \frac{1}{\sqrt{r}}(f_{ij}K_I + g_{ij}K_{II} + h_{ij}K_{III}) \tag{5.1}$$

$$u_i = \frac{1}{G}\left(\frac{2r}{\pi}\right)^{\frac{1}{2}}(f_iK_I + g_iK_{II} + h_iK_{III}) \tag{5.2}$$

where r is the distance from the crack tip, f_i, g_i, h_i, f_{ij}, g_{ij} and h_{ij} are known function of θ and, finally, G is a material property.

In the displacement approach, substituting the displacement field solution in equation 5.2 for certain values of θ along a radial line emanating from the crack tip, allows a plot of K_I, K_{II}, K_{III} against the radial distance r to be drawn. Then by disregarding the results for points very close to the crack tip, the solution can be extrapolated to r = 0 using linear regression method. In the stress approach the same procedure is applied through equation 5.1. These approaches can be employed using either conventional finite elements or with crack tip singularity elements included in the crack zone.

Many authors [32,35,36] have shown that the $\theta = 180°$ line displacements produce accurate and more consistent results than other radial lines and, therefore, the $\theta = 180°$ line displacements are used throughout this study.

5.5 RESULTS AND DISCUSSION

The stress intensity factors *(K_I)* are computed by using the $\theta = 180°$ line nodal displacements and are plotted for various values of r as shown in Figure 5.4 for a crack length *a =1.76 inch.* Results are compared with those of the standard CCT specimen in the same figure. By disregarding the results for points very close to the crack tip, the solution is extrapolated to $r = 0$ using the linear regression. The FE results of the sub-models have

suggested that the crack opens at 90° to 180°, and closes from 270° to 0° due to the nature of the boundary conditions specified in Chapter 2. The opening and closing of the crack is shown in Figure 5.5.

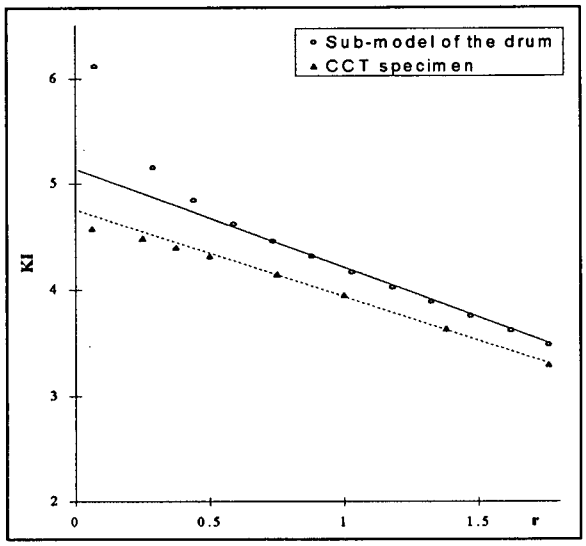

Figure 5.4: K_I vs. r values from FE sub-model and CCT specimen.

The results at different angular positions for a specific crack length are compared to get the variation of stress intensity factor ($\Delta K_I = |K_{I\,max} - K_{I\,min}|$) for each load cycle and the fatigue crack propagation rate for the structure is computed based on the obtained ΔK_I for each crack length as shown in Table 5.1. The crack propagation pattern is assumed to be following Paris Law [37]:

$$\frac{da}{dN} = C \cdot (DK_I)^m \quad \text{or} \tag{5.3}$$

$$N = \int_{c1}^{c2} \frac{1}{C \cdot (DK_I)^m} da \tag{5.4}$$

where:

da/dN is the crack growth rate,
ΔK_I is the variation of stress intensity factor for each load cycle,
N is the number of cycles for the crack to grow from length c1 to length c2,

C, m are material parameters, a function of environment, temperature, etc.

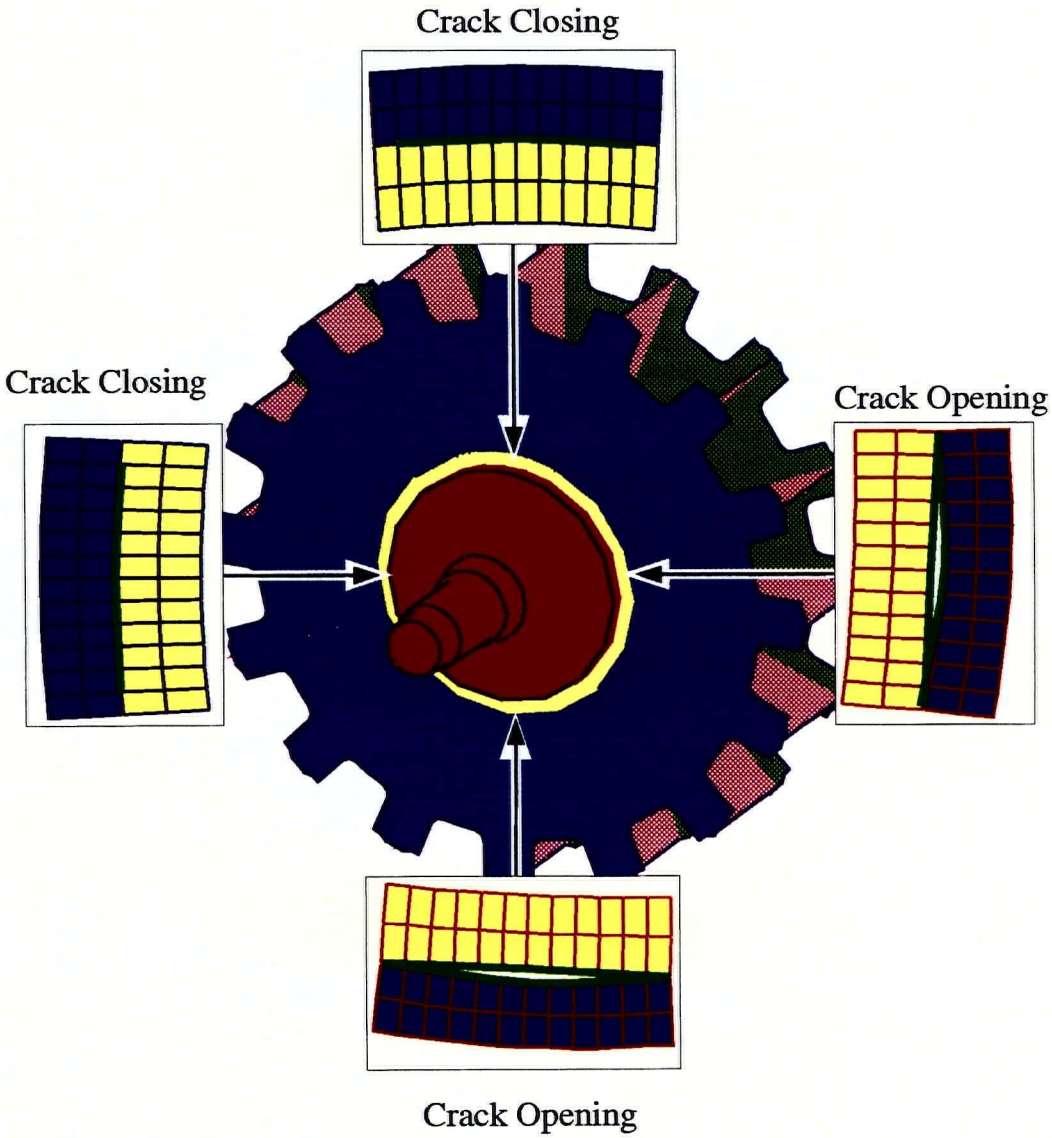

Figure 5.5: Illustration of the crack opening and closing on the sub-model

Table 5.1 Fatigue crack propagation rates

Crack length (Δa, in)	**ΔK_I**	**ΔN (10^6 cycle)**	**N (10^6 cycle)**
(0.29, 0.59)	3.1	29.8	29.8
(0.59, 0.88)	3.7	16.4	46.2
(0.88, 1.18)	4.2	10.8	57.1
(1.18, 1.47)	4.6	8.2	65.4
(1.47, 1.76)	4.8	7.2	72.7

The predicted fatigue life from the above results is plotted in Figure 5.6. As discussed above, it is common practice for engineers to predict the service life of a complicated structure using a standard crack model (can model). The procedure involve FE analysis of the structure with no cracks, and the ΔK_I values are computed based on the obtained alternating stress in the critical or problem area. In this study, the maximum alternating stress value from the full model with no cracks is shown to be 18.62 MPa (2.7 ksi) at the hub to end-plate weldment. Using this stress value with a standard crack model and an initial crack length of 0.59" gives a predicted service life of 90 years according to the analytical solution of a CCT specimen. The results are plotted with those obtained from using FE sub-models in Figure 5.6. The crack length (a) is assumed to be propagating from 0.59" to 1.76" in this study.

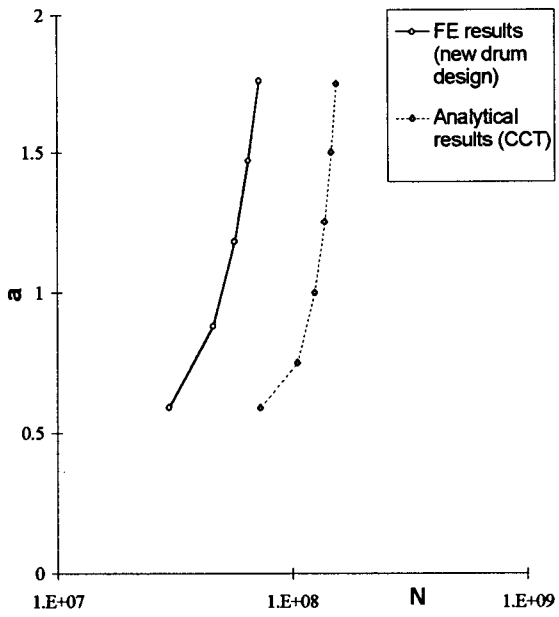

Figure 5.6: Fatigue Cycle of the drum based on FE sub-model and CCT specimen.

Table 5.2 summarizes results of the fatigue life predictions of the structure using the following two methods:

i. ΔK_I values calculated from the alternating stress level of the full FE model and the analytical solution for a CCT specimen,

ii. ΔK_I values calculated with an actual simulation of the crack in the real geometry and under real life loading conditions.

Table 5.2: Comparison of the Fatigue Life Predicted by the Two Methods

Model	**CCT specimen with FE stress results**	**FE model with actual crack**
Service Life	~90 years	~50 years

Assuming an initial crack size of 0.59", the CCT specimen (can-model) shows an approximate life of 90 years for the drum while the actual simulation of the crack using detailed sub-models produces a drum life of approximately 50 years. The comparison has suggested that the fatigue life prediction of the pressure washer drum using a CCT analytical solution may over-estimate the service life of such structure by approximately 80%. It also indicates that common engineering practice of predicting fatigue life of a structure under complicated loading using a standard crack model is non-conservative.

5.6 FATIGUE LIFE PREDICTION OF THE EXISTING DRUM

At this stage, it is thought useful to predict the fatigue life of existing drum design and compare it to the fatigue life of the new design. Since the effort in building a detailed sub-model for the existing design is quite intensive, it was decided to perform the analysis using standard available crack models and the finite element stress results with no crack. This is

thought to be adequate for comparison purposes. The life prediction using a standard through thickness crack model and Paris Law are plotted in Figure 5.7. As indicated from the figure, the service life of the existing design and the new design are estimated to be approximately 9 months and 90 years, respectively. The service life of the structure is extended significantly due to the much lower stress level of the new drum design.

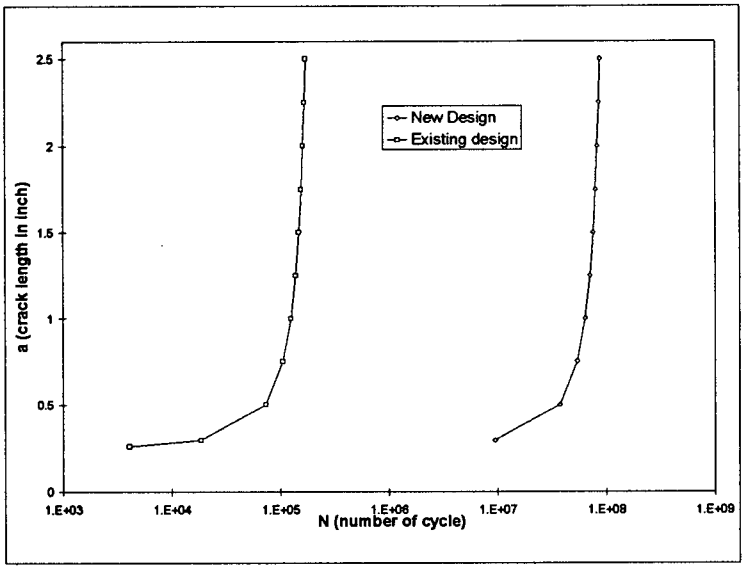

Figure 5.7: Fatigue cycles of the existing and new design

Chapter 6

TRANSIENT HEAT TRANSFER AND THERMAL STRESS ANALYSIS

6.1 INTRODUCTION AND PROBLEM STATEMENT

During the normal start-up process for a pressure washer, the washer drum is heated up to its operating temperature which is about 100°C (210°F). This is normally achieved by partially immersing the drum in a hot bath and rotating it under no load for a given period of time.

The new drum design presented here mainly consists of two main structural components; thin flat or curved plates and a massive solid hub at both ends. It is believed that the stainless steel thin plates will tend to heat up and reach the temperature of the hot bath much faster than the solid hub. Thermal stresses or thermal shock may develop, therefore, at the interface between the plates and the hub. An appropriate start-up procedure is, therefore, required in order to reduce the impact of the thermal shock to the new drum design. The procedures involve examining thermal stresses in critical weld areas of the drum due to the thermal shock loading. Various heat-up scenarios are examined to determine the impact on the stress pattern. The procedure for conducting the analysis in HEAT2 [8]; the transient heat transfer module of NISA family, will be described and an outline of the cases examined, followed by a summary of results obtained for these cases will be given in this chapter.

6.2 THE HEAT TRANSFER MODEL

To obtain the thermal stresses for such problem, the analysis is performed in two sepa

rate stages. First, a heat transfer model is created and analyzed to generate the field solution of nodal temperatures. This is a transient conduction heat transfer analysis with convection boundary conditions that are varying with time due to the rotation of the drum. The only DOF in this analysis is the nodal temperatures; i.e., one DOF per node. The second stage of the analysis will be to use the calculated nodal temperatures, from the first stage, to perform a thermal stress analysis. The FE models used in both stages are basically the same with the difference of the type of analysis and the DOF per node in each case. The procedures are identified in the following steps:

- Generate a FE model using special heat transfer elements (1 DOF per node; the temperature) for the transient heat transfer analysis.
- Apply appropriate boundary conditions. All drum faces immersed or exposed to the hot bath will have a convection boundary condition. Detailed discussion of the boundary conditions is given in the next section.
- Perform transient heat transfer analysis and extract temperature distributions at various time steps.
- Examine temperature distributions to identify a critical one to use for thermal stress analysis. In this step, more than one critical temperature distribution may be identified.
- Use nodal temperatures obtained from the heat transfer analysis as input to the structural model which consists of regular static analysis FE elements. This is the same heat transfer model with different element identification.
- Process the structural model using linear static analysis option to calculate the thermal stress profile.

It is important to note, at this stage, the very limited availability of heat transfer analysis results and data for rotating structures. Solutions to only very limited cases and simple structures are available in literature. As an example, Eriksson and Sunden [38,39] have developed special numerical formulation that provides transient temperature distribution in a rotating cylindrical shell heated by time varying flux. It is obvious that such simple cases will not be appropriate to give a good approximation to the drum case.

6.3 BOUNDARY CONDITIONS

Convection is the only boundary condition applied to the model in this analysis. Six transient heat transfer runs are processed simulating different convective boundary conditions (defined by different time amplitude curves and film coefficients). Variation in heat transfer or film coefficient is intended to simulate stationary and rotating drum conditions. The variation in the time amplitude curve is intended to simulate the variation in heat transfer coefficient during drum rotation. The load cases considered involve increasing the number of hot bath temerature steps that the drum will be exposed to in order to reach the final operating temperature as shown in Figure 6.1. This multi-step approach is thought to reduce the thermal gradient between the plates and the solid hub and, therefore, minimize thermal stresses.

6.4 HEAT TRANSFER ANALYSIS RESULTS

Sample results for the cases discussed above are given in this section. The thermal stress along the hub and end-plate intersection (for a single stage heating) is shown in Figure 6.2 whereas the corresponding temperature and stress values are given in Figure 6.3.

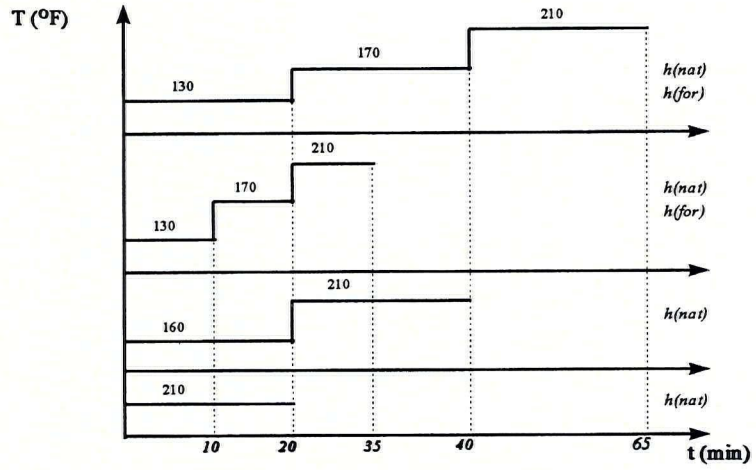

Figure 6.1: Various heat-up curves for start-up conditions

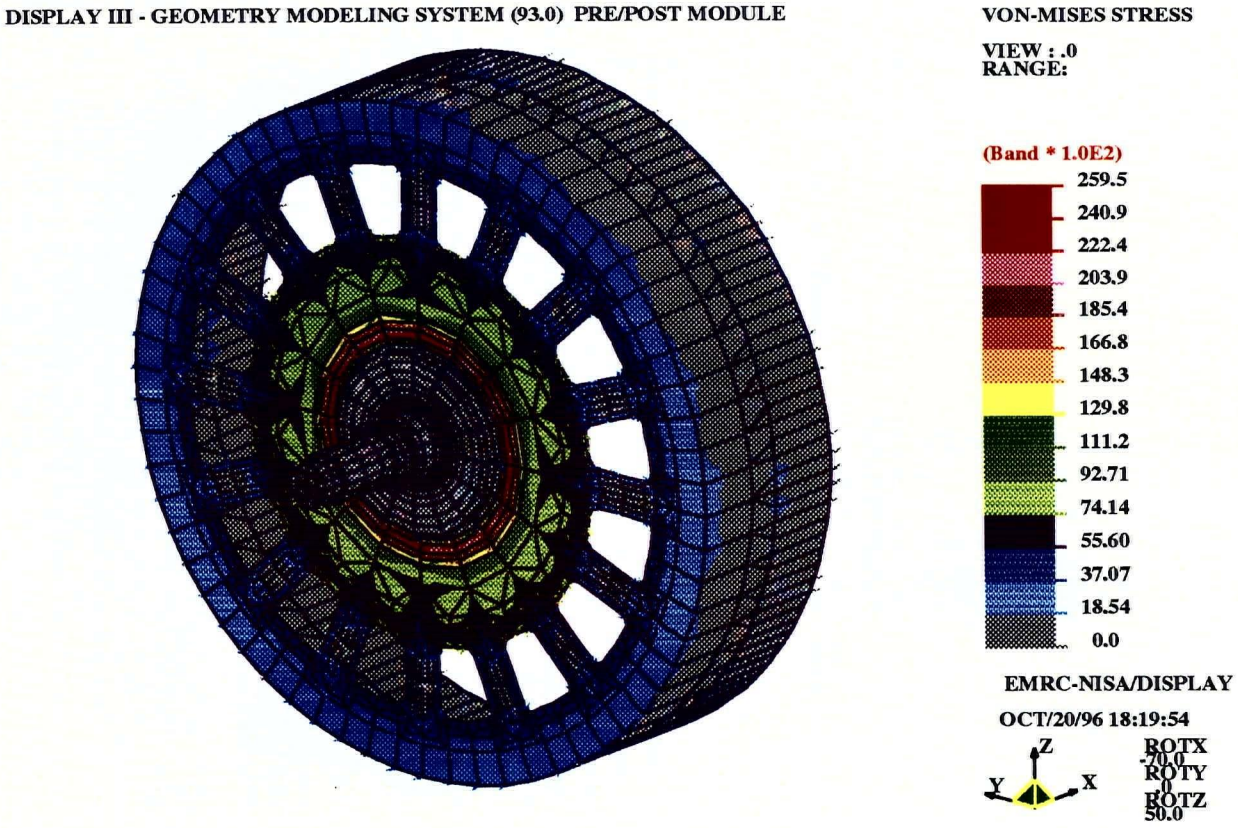

Figure 6.2: Stress contours of the end component for single stage heating

Most of the results for various heat-up schemes are summarized and presented in Figure 6.3 and 6.4. The maximum stress values along the end-plate and hub weldment are given in Table 6.1. The improvement among the models with different heat-up curves are also presented in the same table. As indicated in Figure 6.4, the weldment between the end-plate and hub is the most critical area in terms of thermal stress level due to the rapid change of thickness in this area. The static analysis indicated that the worst thermal stress level comes with the single stage heating. The stress level of the end-plate/ hub intersection may be substantially reduced by inducing more steps in the heat-up cycle.

Table 6.1: Comparison of thermal stress levels

	1-step	**2-step (20 min/step)**	**3-step (10 min/step)**	**3-step (20 min/step)**
Stress Level	23 ksi	19.5 ksi	19.5 ksi	18.5 ksi
Critical time step	within 5 min.	after 25 min.	after 25 min.	after 45 min.
Improvement	---	15%	15%	20%

The quoted stress values are the maximum stress level that occurred during the heating period. The analysis has demonstrated that, as predicted, maximum stresses are due to a single step heating case. For this case, the peak stress level is reached within the first 5 minutes of heating. For the two-step heating scheme, the peak stress is reached 5 minutes after the start of the second stage heating and the stress level has shown 15% improvement (i.e., reduction) over the single-step heating. For the three-step case, the maximum stress is reached at 5 minutes after the start of the third stage and a further 5% improvement is achieved over the two-step heat-up cycle.

All stresses are unaveraged von-Mises stress in ksi
Quoted stresses are the maximum of the shell layers

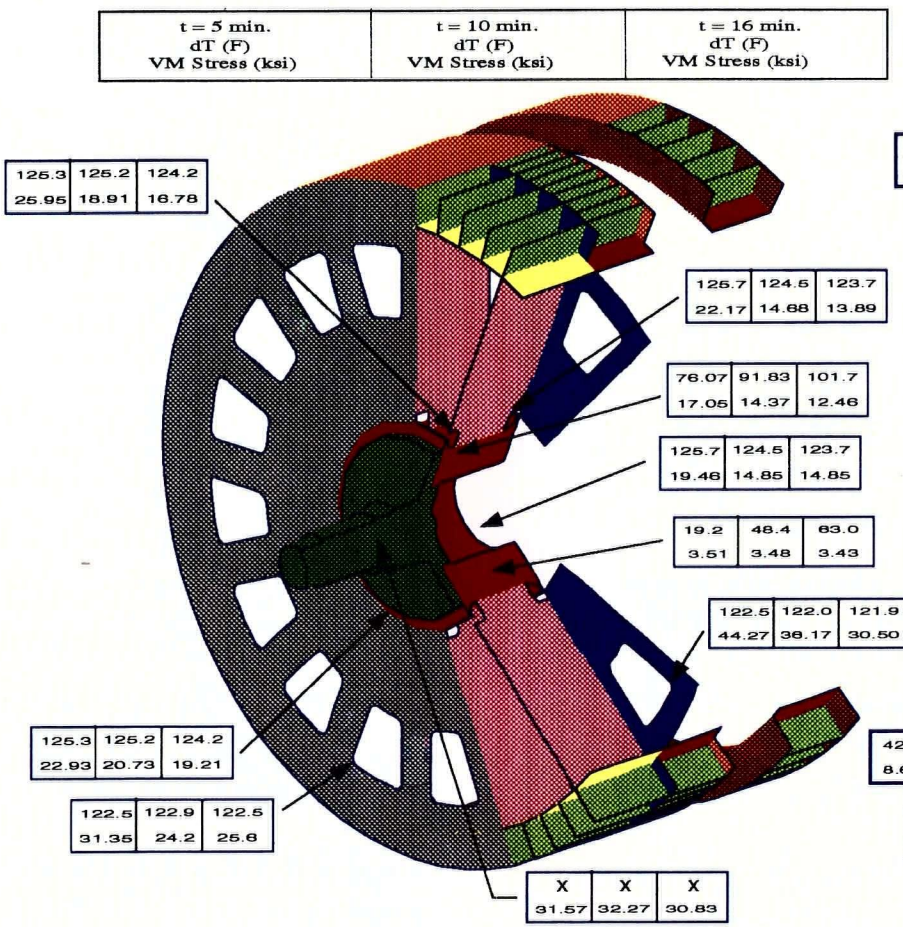

Figure 6.3: Temperature and stress results for the single step heat-up curve

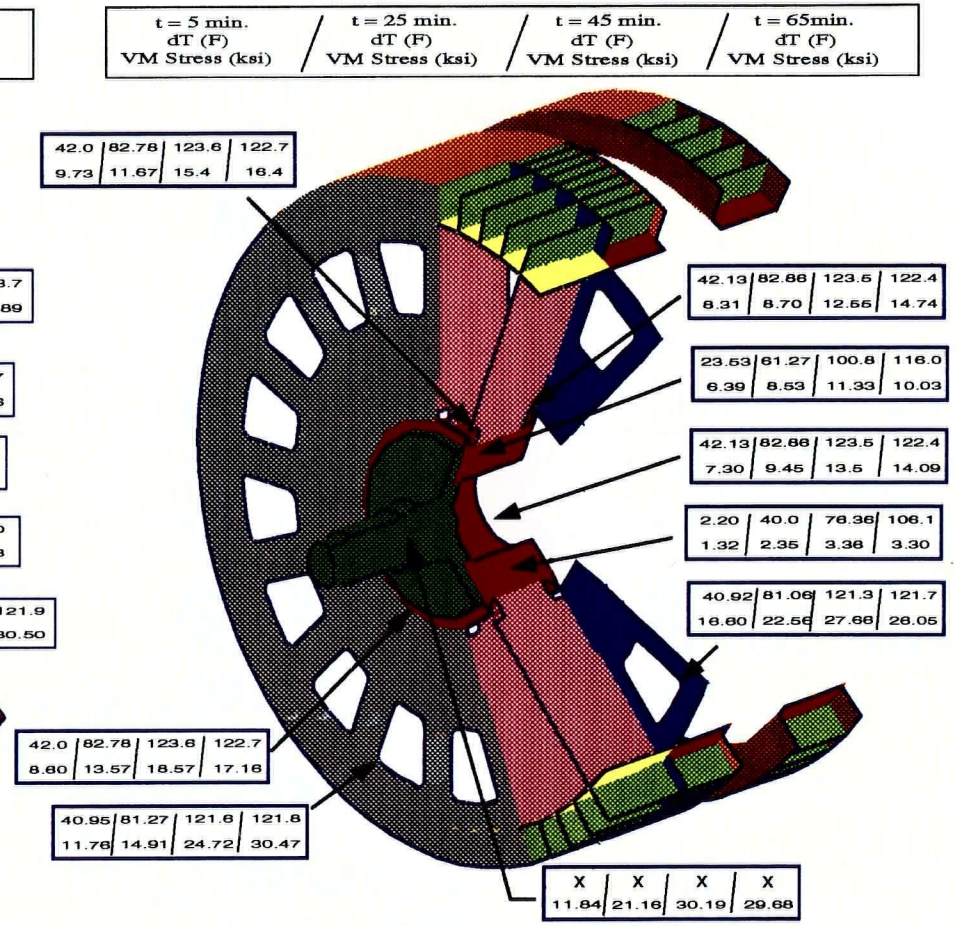

Figure 6.4: Temperature and stress results for the 3-step (20min./step) heat-up curve

The results suggest that increasing the number of steps in the heat-up cycle is beneficial to the thermal stress level but a certain amount of waiting time is required in each increment. It is also shown that the plates will reach the bath temperature in a very short time, probably within 5 minute whereas the solid hub will need more than 30 minutes to reach the same temperature. This may explain why the three-step heat-up cycle (with 10 min. for each step) does not show improvements over the two-step case.

A concern is raised that the thermal stress cycles due to the start-up conditions may have an impact on the fatigue life of the drum. To examine this concern, a very conservative start-up conditions are assumed. These conditions includes a start-up frequency of 2 time per month with a fully alternating stress of 18.5 ksi. By using a standard crack model in an infinite plate, a life of 480,000 cycles or 20,000 years is obtained. Using Miners rule to assess the damage shows that superimposing the thermal cycles on the existing operating stress will only reduce the 90 years life expectancy estimate to 89.6 years.

6.5 RECOMMENDATION

The analysis has shown that increasing the number of steps of preheating the drum will be beneficial and it has also shown that a proper amount of waiting time is required in order to minimize the thermal stress within the structure during the start-up process. A heat-up cycle that consists of three or more increments of heating, with a holding period of at least 20 minutes are thus recommended for normal start up procedure.

Chapter 7

CONCLUSIONS

The problem of the short service life of pressure washer drums used in the pulp and paper industry is addressed. A new design that substantially reduces the stress levels in the drum and increases life expectancy is presented and analyzed in this thesis.

Experimental testings were carried out to determine the load carrying characteristics and critical boundary conditions of the pressure washer drum. Shape optimization of a specific area of the new washer drum was carried out using finite element optimization capabilities. A lighter design with appropriate stress level is achieved. The procedure and results of the sub-modeling method for the shape optimization are discussed. To further reduce the risk of fatigue cracking, X-ray examination of the critical hub to end-plate welds is performed. Stress-relief of the entire end component is also performed. A prototype of the new drum design was built and showed encouraging reliability in the past 20 months of operation in the Red Rock pulp mill in Ontario, Canada.

The service life of the washer drum is predicted by using a standard crack model, and a detailed FE study for crack propagation at the critical area. Obtained results show significant impact of the method of analysis on the predicted life of the component. The comparison has suggested that the common engineering practice of predicting the fatigue service life of a structure using a simplified crack model may be non-conservative.

A special start up procedure that minimizes thermal shock to the structure is proposed and the transient heat transfer analysis performed during this study has suggested that the new procedure provides significant improvement in the thermal stress level.

REFERENCES

[1] J.K. Perkins and K.M. Jackson, "The washing of brown stock", In: Brown Stock Washing Using Rotary Filters, Ed. J.K. Perkins, TAPPI press, (1983) 1-6.

[2] J.A. Perkins, "Rotary filter washing equipment", In: Brown Stock Washing Using Rotary Filters, Ed. J.K. Perkins, TAPPI press, (1983) 6-10.

[3] G.A. Smook, Handbook for pulp and paper technologists, Angus Wilde Publications, Vancouver , BC, Canada (1992).

[4] C.R. Morin and J.P. Sheehan, "Stress corrosion cracking problems in the pulp and paper industry", In: Corrosion-76; Proc. of the Int. Corrosion Forum, Pub. by the National Assoc. of Corrosion Engnrs., (1976) Paper#52.

[5] H.K. Bhadeshia, "Modeling of steel welds", Material Science and Technology, 8 (1992) 123-133.

[6] K.J. Bathe, Finite element procedures, Printice Hall, Englewood Cliffs, N.J. (1993).

[7] O.C.Zienkiewicz, The finite element Method 3nd Ed., McGraw-Hill Book Company Ltd. (1977).

[8] NISA user's manual, Engineering Mechanics Research Corporation. Troy, Michigan, USA (1993).

[9] NISA verification problems manual, Engineering Mechanics Research Corporation. Troy, Michigan, USA (1993).

[10] DISPLAY III user's manual Vol 1&2, Engineering Mechanics Research Corporation. Troy, Michigan, USA (1993).

[11] M.Taylor, M.S.Gadala and G.Hodgins, New design for pressure washer drums, US patent, serial no. 5582728, issuing date: Dec.1996.

[12] J.M. Vitek and S.A. David, "The solidification and aging behavior of types 308 and 308 CRE stainless steel welds", Welding Research Supplement, 63 (1984) 246s-253s.

[13] B. Gretoft, S. Rigdal, L. Karlsson and L.E. Sevensson, "Influence of welding process on mechanical properties of duplex stainless steel weld metals, In: Stainless Steels-87, Institute of Metals, (1988) 105-107.

[14] M.S. Gadala, S. Fok and M. Tayler, "Design modifications and experimental testing for pressure washer drum", submitted for publication to TAPPI J., (1996)

[15] Report #94-TS031R, "Strain gauge results from pressure washer drum experiment", SciMech Technical Services, (1994).

[16] Report #95-TS052R2, "Strain gauge results from TRIDOM washer drum operation", SciMech Technical Services, (1995).

[17] "Stainless Steels" ; ASM Specialty Handbook, ASM International, Materials Park, OH, (1994).

[18] G.S. Sangdahl, "Stress relieving of austenetic stainless steels", Metals Progress, v 86 n 2, (1964) 100-104.

[19] "Heat treating of stainless steels", Published by: ASM committee on heat treating of stainless steels, ASM International, Materials Park, OH, (1966).

[20] W.Smith, Structure and properties of engineering alloys 2nd Ed., McGraw-Hill Book Company Ltd. (1993).

[21] NISAOPT User's manual, Engineering Mechanics Research Corporation, Troy-Michigan, (1993).

[22] Tracey, "Finite element for three-dimension elastic crack analysis", *Nucl. Engng Design* 26 (1974) 282-290.

[23] W.Blackburn, "Calculation of stress intensity factors at crack tips using special finite elements", in *Mathematics of Finite elements*, academic press, NY (1973) 327-336.

[24] R.Barsoum, "On the use of isoparametric finite elements in linear fracture mechanics". *Int. J. numer. Meth Engng* **10** (1976) 25-37.

[25] X.B.Lin and R.A.Smith, "Numerical prediction of fatigue crack growth of a surface defect". *Fatigue Fract. Engng Mater. Struct* Vol.18 No.2 (1995) 247-256.

[26] T.Boukharouba, C.Chehimi, J.Gilgert and G.Pluvinage, "Behaviour of semi-elliptical cracks in finite plates subjected to cyclic bending". *Handbook of fatigue crack propagation in metallic structures*, Elsercier Science B.V. (1994) 707-731.

[27] M.S. Gadala, S.Fok and M. Tayler, "Analysis and design of pressure washer drums for pulp and paper industry", submited to The third conference on fracture & strength of solids, Hongkong University of Science & Technology. (1997)

[28] H.Liebowitz and E.T. Moyer,Jr., "Finite element methods in fracture mechanics", *Composites and Structures* Vol.31, No.1 (1989) 1-9.

[29] S.K.Chan, I.S.Tuba and W.K.Wilson, "On the finite element method in linear fracture mechanics", *Engng Fracture Mech* **2** (1970) 1-17.

[30] C.A.Hall,M.Raymund and S.Palusamy, *Int. J. of Fracture*, Vol 15 (1979) 231.

[31] W.K.Wilson, "On combined mode fracture mechanics", Ph.D. thesis, University of Pittburgh, PA (1969).

[32] D.M.Tracy, "Finite elements for determinaton of crack tip elastic stress intensity factors", *Engng Fracture Mech.* **3** (1971) 225.

[33] R.Henshell and K.Shaw, "Crack tip finite elments are unnecessary", *Int. J. Num. Meth. Engng.* **9** (1975) 495.

[34] Raju and J.C.Newman,Jr, "Three dimensional finite element analysis of finite thickness fracture specimens", NASA TN D-8414 (1977).

[35] A.J.Fawkes, D. Owen and A. Luxmoore, "An assessment of crack tip singularity models for use with isoparametric elements", *Engng Fracture Mech.* **11** (1979) 143.

[36] R.Gallagher, "Numerical methods in fracture mechanics", *Proc. Of the 1st. Int. Conf.*, Pineridge Press, Swansea (1978) 1.

[37] Paris, "The fracture mechanics approach to fatigue. Fatigue-an interdisciplinary approach", *Proc. 10th Sagamore Army Mat. Res. Conf.* Syracuse University Press (1964) 107.

[38] B.Sunden, "Transient Conduction in a cylindrical shell with time-varying incident surface heat flux and convective and radiative cooling", *Int. J. Heat Mass Transfer*, Vol.32, No.3 (1989) 575-584.

[39] D.Eriksson and B.Sunden, "Transient conduction in a rotating cylinderical shell exposed to an incident time varying heat flux", In Advanced Computational Methids in Heat Transfer III, Computational Mechanics Publications, Southampton (1994) 3-10.

APPENDIX

Calculation of the equivalent stiffness and density of the perforated deck shell

Plate type: 3/8" Staggered (0.375" diamater, 33% open)

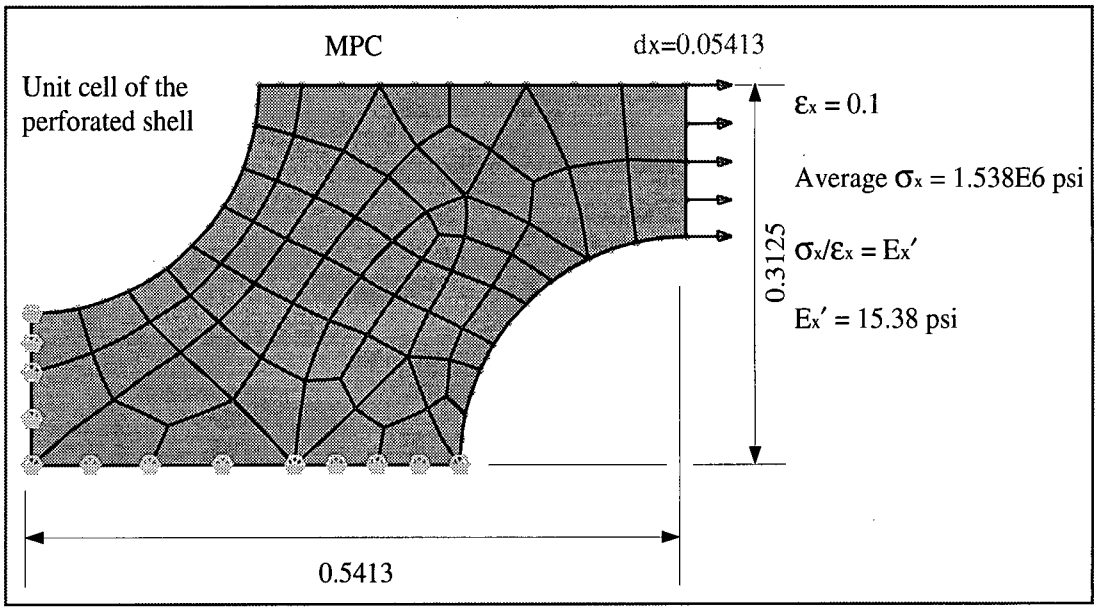

dx, dy applied displacement MPC : Multi-point Constraint Equation

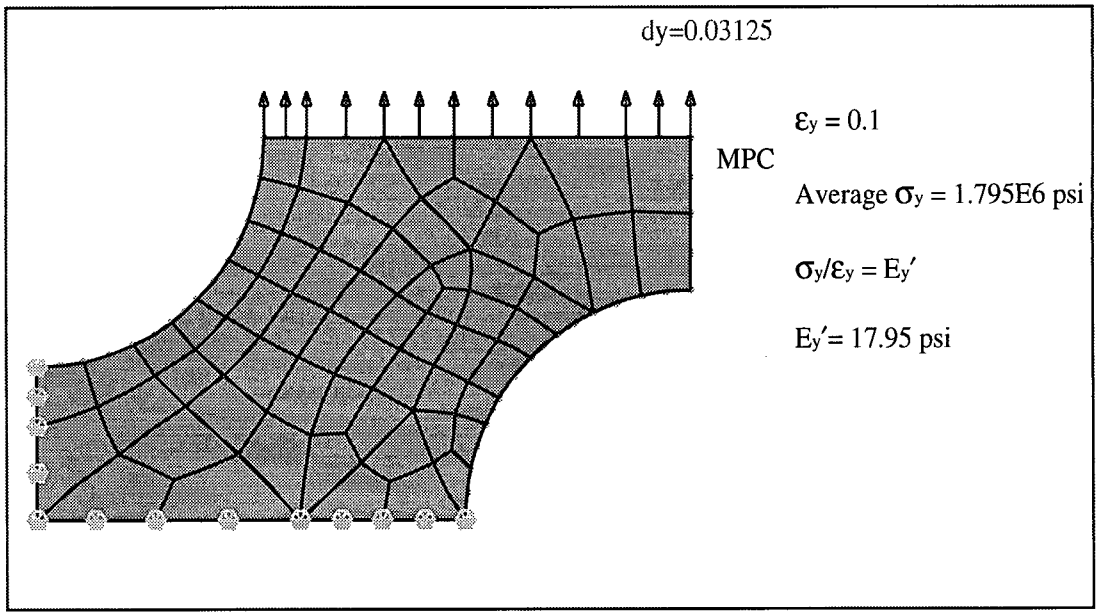

equivalent young's modulus: E′ = average (Ex′ , Ey′) = 1.67E7 psi

equivalent density: ρ′ = 33% * 7.41E-4 = 4.965E-4 lbf sec^2/in^4

7.41E-4: density of solid stainless steel